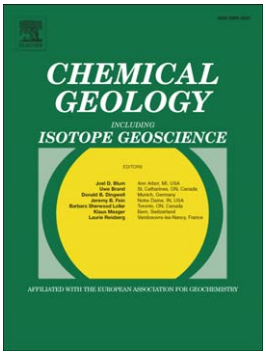

Geochemical variations in the Central Southern Volcanic Zone, Chile (38-43°S): The role of fluids in generating arc magmas

G. Jacques, K. Hoernle, J. Gill, H. Wehrmann, I. Bindeman, Luis E. Lara

PII: S0009-2541(14)00056-4
DOI: doi: 10.1016/j.chemgeo.2014.01.015
Reference: CHEMGE 17134

To appear in: *Chemical Geology*

Received date: 2 September 2013
Revised date: 20 January 2014
Accepted date: 27 January 2014

Please cite this article as: Jacques, G., Hoernle, K., Gill, J., Wehrmann, H., Bindeman, I., Lara, Luis E., Geochemical variations in the Central Southern Volcanic Zone, Chile (38-43°S): The role of fluids in generating arc magmas, *Chemical Geology* (2014), doi: 10.1016/j.chemgeo.2014.01.015

Geochemical variations in the Central Southern Volcanic Zone, Chile (38-43°S): The role of fluids in generating arc magmas

G. Jacques[1]*, K. Hoernle[1,2], J. Gill[3], H. Wehrmann[1], I. Bindeman[4], Luis E. Lara[5]

[1]Collaborative Research Center (SFB574), University of Kiel and GEOMAR, 24148 Kiel, Germany

[2]GEOMAR Helmholtz Centre for Ocean Research, 24148 Kiel, Germany

[3]University of California, Santa Cruz CA 95064, USA

[4]University of Oregon, Eugene OR 97403, USA

[5]Servicio Nacional de Geología y Minería, Santiago, Chile

*Corresponding author:

Dr. Guillaume JACQUES

GEOMAR Helmholtz Center for Ocean Research Kiel

Wischhofstraße 1-3

24148 Kiel Germany

gjacques@geomar.de

Telefon: +49 (0) 4 31 600 25 61

Fax: + 49 (0) 4 31 600 2915

Abstract

We present new Sr-Nd-Pb-Hf-O isotope data from the volcanic arc (VA, volcanic front and rear arc) in Chile and the backarc (BA) in Argentina of the Central Southern Volcanic Zone in Chile (CSVZ; 38-43°S). Compared to the Transitional (T) SVZ (34.5-38°S; Jacques et al., 2013), the CSVZ VA has erupted greater volumes over shorter time intervals (Völker et al., 2011) and produced more tholeiitic melts. Although the CSVZ VA monogenetic cones are similar to the TSVZ VA samples, the CSVZ VA stratovolcanoes have higher ratios of highly fluid-mobile to less fluid-mobile trace elements (e.g. U/Th, Pb/Ce, Ba/Nb) and lower more- to less-incompatible fluid-immobile element ratios (e.g. La/Yb, La/Sm, Th/Yb, Nb/Yb), consistent with an overall higher fluid flux and greater degree of flux melting beneath the CSVZ stratovolcanoes compared to the CSVZ monogenetic centers and the TSVZ VA. The CSVZ monogenetic centers overlap the TSVZ in Sr and Nd isotopes, but the stratovolcanoes are shifted to higher Sr and/or Nd isotope ratios. The Pb isotopic composition of the CSVZ overlaps the TSVZ, which is clearly dominated by the composition of the trench sediments, but the CSVZ monogenetic samples extend to less radiogenic Pb isotope ratios. $\delta^{18}O_{melt}$ from the CSVZ stratovolcano samples are below the MORB range, whereas the CSVZ monogenetic and the TSVZ samples fall within and slightly above the MORB range. The Nd and Hf isotopic ratios of the CSVZ VA extend to more radiogenic compositions than found in the TSVZ VA, indicating a greater contribution from a more depleted source. These correlations are interpreted to reflect derivation of fluids from hydrothermally altered oceanic crust and/or serpentinized upper mantle of the subducting plate. CSVZ BA basalts largely overlap TSVZ BA basalts, displaying less or no subduction influence compared to the VA, but some CSVZ BA basalts tap more enriched mantle, possibly

subcontinental lithosphere, with distinctively lower Nd and Hf and elevated $^{207}Pb/^{204}Pb$ and $^{208}Pb/^{204}Pb$ isotope ratios.

Keywords: Subduction zone, Chilean Southern Volcanic Zone, fluids, Sr-Nd-Pb-Hf-O isotopes, Argentinian backarc, arc basalts

Words: 316

1. Introduction

Along-arc variation in the composition of magma is typical for many subduction zones, and can be related to many factors. For example, there can be a change in the composition of subducting sediment or oceanic crust or both. Erosion can vary as a function of rainfall, glaciation and relief, resulting in a variable thickness and proportion of continentally-derived trench sediment. The subducting oceanic crust can vary in age and therefore slab surface temperature and degree of alteration, and in composition depending on the ocean ridge at which it formed. The mantle wedge can be heterogeneous in trace element and isotope ratios.

The tectonic setting can also change along strike, and can influence the ascending magmas. Thicker crust increases the potential for assimilating upper crustal material into the melts, and can affect the depth and extent of crystal fractionation. The presence of large fracture zones or bend-faults on the subducting plate may increase the potential for hydration of the lower oceanic crust and/or serpentinization of the underlying lithospheric mantle. The geometry of the slab (depth, dip) can also vary. If the slab beneath the volcanoes is deeper, it will be hotter and is

therefore more likely to melt rather than dehydrate, increasing the potential for recycling incompatible elements such as Th, Nb, Ta, Hf and Zr. Finally, there can be differences in the role of sediment accretion versus erosion in the forearc, which affects the amount of sediment and upper and lower continental crust being subducted.

All of the above variables change along the Chilean margin. In order to evaluate these variables, this study focuses on the volcanic arc of a portion of the Southern Volcanic Zone (SVZ) of Chile and the backarc in Argentina between 38°S and 43°S. Together with major and trace element data from Wehrmann et al. (2014, and in rev), our new Sr-Nd-Hf-Pb-O isotope data provide a comprehensive new geochemical data set for this area. Combining geochemical, morphological and geophysical data, we compare and contrast cinder cone and stratovolcano samples from the Central SVZ (CSVZ: 38-43°S) and then compare and contrast the CSVZ with the Transitional SVZ (TSVZ: 34.5-38°S, Jacques et al., 2013) segment in order to identify the source of the main along-strike variations in magma composition.

2. Geological setting and previous geochemical studies

2.1 Geological background

The Andean cordillera is more than 7,500 km long, extending from Colombia to Southern Chile. Volcanism results from the subduction of the Nazca (7-9 cm/year) and the Antarctic (2 cm/year) Plates below the South American Plate (Norabuena et al., 1998; Angermann et al., 1999). The Andes volcanic arc has four active volcanic segments, divided by volcanic gaps. Volcanism occurs when the slab dip angle is greater than 25° (Stern, 2004). The segments have

been named the Northern Volcanic Zone (NVZ; 5°N-2°S) in Colombia and Ecuador, the Central Volcanic Zone (CVZ; 16-28°S) in Peru and northern Chile, the Southern Volcanic Zone (SVZ, 33-46°S) in Central Chile, and the Austral Volcanic Zone (AVZ; 49-54°S) in southern Chile.

The SVZ in Chile consists of more than 60 Quaternary volcanoes, three silicic caldera systems, and numerous minor eruptive centers (Stern, 2004, Figure 1a). The SVZ has been divided into the Northern Southern Volcanic Zone (NSVZ; 33°-34.5°S; e.g. Hildreth and Moorbath, 1988), the Transitional Southern Volcanic Zone (TSVZ; 34.5-37°S; e.g. Tormey et al., 1991), the Central Southern Volcanic Zone (CSVZ; 37.0-41.5°S; e.g. Hickey et al., 1984, 1986, Hickey-Vargas et al., 1989) and the Southern Southern Volcanic Zone (SSVZ; 41.5-46°S; e.g. Naranjo and Stern, 2004), based on the geochemical characteristics of the erupted rocks (see also López-Escobar et al., 1995). Dungan et al. (2001) suggested a different division: the Tupungato-Maipo Segment (TMS, 33°-34.2°S), the Palomo-Tatara Segment (PTS, 34.7°-36°S), and the Longaví-Osorno Segment (LOS, 36.2°-42°S) (see also Sellés et al., 2004).

This study focuses on the SVZ volcanoes between 38-43°S, which we collectively refer to as the CSVZ (Figure 1b). CSVZ volcanic arc (VA, including both the volcanic front and rear arc) studied volcanoes are Lonquimay, Llaima, Villarrica and two nearby cluster of cinder cones (Huelemolle and Caburga), Mocho-Choshuenco, Casablanca, Osorno and the monogenetic cones of Cabeza de Vaca (Cayutue cluster). Apagado and Minchinmávida-Chaitén, sometimes included in the SSVZ, are here included in the CSVZ.

We separate the stratovolcanoes from the monogenetic cones because they differ in geochemistry as well as morphology (see Section 5.2). The southernmost samples come from small cinder cones in the area of Minchinmávida-Chaitén. Apagado is also a big cinder cone near two stratovolcanoes (Yate and Hornopirén).

The CSVZ segment includes some of South America's most active volcanoes (e.g. Llaima and Chaitén erupted in 2008, Cordón-Caulle in 2011), including Villarrica considered to be amongst the most active volcanoes in South America (with annually recurrent activity since 2008). The CSVZ has also had the highest magma extrusion rate of the SVZ (NSVZ (33-34.5°S) = 3.8 km^3/km/Ma, TSVZ (34.5-37°S) = 4.2 km^3/km/Ma, CSVZ (37-42°S) = 14.9 km^3/km/Ma, SSVZ (42-43°S) = 2.6 km^3/km/Ma) (Völker et al., 2011).

The CSVZ backarc (BA) in Argentina extends from 70 km to 230 km behind the CSVZ VA. This region is part of the large Patagonian volcanic province which was active from the Tertiary to Recent (Kay et al., 2004). We sampled a number of Holocene cinder cones from two different regions and from isolated lava plateau (Kay et al., 2004, 2007). Our northernmost BA samples come from the southern part of the Loncopué Graben near Copahue volcano (ca. 38-39°S) (Varekamp et al., 2010). Our southernmost BA samples come from the Crater Basalt Volcanic Field (700 km^2) which produced Quaternary lavas and tephras (600-340 ka; Pécskay et al., 2007).

The Nazca Plate currently subducting north of the Valdivia fracture zone (40°S) formed at the East Pacific Rise (EPR) whereas the plate further south formed at the Chile Ridge (Herron et al., 1981; Tebbens and Cande, 1997; Tebbens et al., 1997). The age of the incoming plate ranges from 14 Ma south of the Chiloé fracture zone at 42°S, to 25 Ma south of the Mocha Fracture Zone at 38°S. More fracture zones with more pronounced morphology and multiple splays are present in the slab subducting beneath the CSVZ compared to the NSVZ and TSVZ (Figure 1), where only the rather minor Mocha fracture zone subducts. There are also more numerous bend-faults on the trench outer-rise offshore the CSVZ (Contreras-Reyes et al., 2007). Consequently the potential for hydration of the lower oceanic crust and serpentinization of the

upper mantle of the subducting slab is greater offshore the CSVZ than the TSVZ. Offshore of the CSVZ, the trench is floored by ca. 2.2 km of sediments (Contreras-Reyes et al., 2008) that consist of 100 m of pelagic clays overlain by turbidites and silty clay derived from the continental basement and the arc (Völker et al., 2008; Lucassen et al., 2010; see also Plank, 2011 for sediment description compilation).

The crustal thickness varies from 60 km beneath the NSVZ to 40 km beneath the CSVZ where it remains relatively uniform (Völker et al., 2011). The depth to the surface of the subducting slab beneath the CSVZ is also relatively constant, being located at ca. 130 km beneath the volcanic front north of 41°S and decreasing to ca. 110 km at 43°S (Tassara et al., 2006). The thickness of the overlying mantle wedge and asthenospheric portion of the wedge beneath the CSVZ range from 80 to 100 km and 60 to 80 km, respectively (Tassara et al., 2006; Völker et al., 2011). Throughout the area of this study (38-43°S), the VA eruptive centers lie directly on the Meso-Cenozoic plutonic rocks of the Patagonian batholith (Stern, 2004, Lucassen et al., 2004, Cembrano and Lara, 2009 and references therein).

2.2 Previous geochemical studies

In the CSVZ VA, both stratovolcanoes and cinder cones produce mainly tholeiitic and high-Al basalts and basaltic andesites. Their Sr-Nd-Pb-O and U series isotopes preclude significant assimilation of old sialic crust (e.g. Hickey et al., 1984, 1986, Hickey-Vargas et al., 1989, 2002; Futa and Stern, 1988; Sigmarsson et al., 1990, 2002). Andesites, dacites and rhyolites in the CSVZ have the same isotopic composition as basalts, indicating that they form by fractionation without significant assimilation (Gerlach et al., 1988) or that they only

assimilated crust with a similar isotopic composition such as young plutonic rocks (e.g. McMillan et al., 1989; Reubi et al., 2011). The aforementioned studies concluded that the magmas south of 34.5°S were produced by melting of the subarc mantle wedge contaminated by fluids derived from the dehydration of the subducted oceanic basalts and sediments. Based on correlations between U-series disequilibria and $^{10}Be/^{9}Be$ isotope ratios, Morris et al. (1990) and Sigmarsson et al. (2002) argued that the largest slab signature is observed in the CSVZ, at Villarrica volcano. Finally, Hickey-Vargas et al. (2002) found that the small eruptive centers near Villarrica were depleted in fluid-mobile elements compared to the main edifice.

Several authors have attributed the origin of the CSVZ BA basalts to melting of lithospheric and/or asthenospheric mantle with or without a slab-derived component. Stern et al. (1990) analyzed Pliocene and Quaternary alkali basalts of the Patagonian Plateau (ca. 34-50°S) in the SVZ BA as well as the Austral Volcanic Zone BA further south. They distinguished a "transitional" group that erupted on the western edge of the Andes, versus a "cratonic" group that erupted in the area of the Cenozoic plateau. The "transitional" basalts contain a slab-derived component in their source, whereas the "cratonic" basalts are produced by low degrees of melting of a heterogeneous subcontinental lithospheric and/or asthenospheric mantle. They proposed that the degree of partial melting and the amount of slab-derived component decrease eastward away from the VA. Varekamp et al. (2010) identified an EM-1-like signature in the young, olivine-rich basalts from the Loncopué Graben in the BA, possibly reflecting subcontinental lithospheric mantle. In the Crater Basalt Volcanic Field (BA), volcanic rocks from monogenetic centers were attributed to decompression melting of a garnet lherzolite asthenospheric mantle (Massaferro et al., 2006, Pécskay et al., 2007).

3. Material and analytical methods

The youngest and freshest, generally olivine-bearing volcanic rocks (lava and tephra) were sampled from each selected volcanic area. Their GPS-based locations and age estimate are provided in Supplementary Table 1. During our sampling campaigns, we avoided units containing xenolithic or xenocrystic material in order to minimize the effects of crustal contamination. Samples were later handpicked under a binocular microscope to select only the freshest part of the rock and to avoid xenolithic or xenocrystic material and filled vesicles. Details of the sample preparation, XRF, ICP-MS and isotope analytical methods can be found in Jacques et al. (2013) and Hoernle et al (2008, 2011). The procedures for the isotope analyses are summarized below.

We analyzed Sr, Nd and Pb isotope ratios on ThermoFinnigan TRITON (Sr, Nd) and Finnigan MAT 262-RPQ2+ (Pb) thermal ionization mass spectrometers at GEOMAR. To ensure high precision Pb isotope analyses, we used a double spike method. Errors for Sr, Nd, Pb and Hf measurements are reported at the 2σ confidence level. In order to remove possible surface contamination, 100-150 mg of 0.5-2 mm sized, fresh rock chips were first leached in 2N HCl at 70°C for 1-2 hours and then triple-rinsed with ELGA water. Mass-bias correction for Sr and Nd isotope ratios were done within run to $^{86}Sr/^{88}Sr = 0.1194$ and $^{146}Nd/^{144}Nd = 0.7219$. NBS987 and our in-house Nd SPEX standard were measured every 4th to 5th sample and normalized to our preferred values of $^{87}Sr/^{86}Sr = 0.710250$ for NBS987 and $^{143}Nd/^{144}Nd = 0.511715$ for SPEX (corresponding to $^{143}Nd/^{144}Nd = 0.511850$ for La Jolla, Krolikowska-Ciaglo et al., 2005). We applied the normalization values to the data for each sample. Thereby, possible machine drift over the course of the project (2009-2012) was compensated achieving maximum data

comparability. External 2σ uncertainties did not exceed ± 0.000011 for NBS987 and ± 0.000005 for SPEX (n= 25). The reference material NBS981 was included in each analytical run and the double spike corrected values are $^{206}Pb/^{204}Pb$ = 16.9413 ± 21, $^{207}Pb/^{204}Pb$ = 15.4994 ± 20, $^{208}Pb/^{204}Pb$ = 36.7241 ± 56, $^{207}Pb/^{206}Pb$ = 0.914889 ± 37, $^{208}Pb/^{206}Pb$ = 2.16773 ± 13 (n=38). Our data are in good agreement with published double and triple spike data for NBS981 (see Hoernle et al., 2011). Each sample batch was accompanied by a blank measurement. Total Pb chemistry blanks were below 25 pg (with the exception of a single Pb blank of 200 pg), Sr-Nd chemistry blanks were usually less than 100 pg and 50 pg, respectively. All these blank levels are insignificant with regard to the samples' Pb, Sr, and Nd contents. Replicate analyses of unknowns proved to be within the external 2σ reproducibility of the Sr-Nd-Pb reference materials.

For Hf isotopes, we used a NU Plasma HR MC-ICPMS at GEOMAR. 200-500 mg of 0.5-2 mm sized fresh rock chips were processed according to the protocol reported in Blichert-Toft et al. (1997) and Geldmacher and Hoernle (2006). Samples were diluted prior to analysis to 80-100 ppb Hf to obtain a total Hf beam of 12-14 V. Hf isotope ratios were determined through static multi-collection. Mass-bias correction was performed assuming exponential mass fractionation to $^{179}Hf/^{177}Hf$ = 0.7325. A normalization value for each sample sequence was generated for our in-house Hf standard solution SPEX, which was analyzed every 3 to 5 samples. During the entire project period (2010-2012), the solution yielded $^{176}Hf/^{177}Hf$ = 0.282170 ± 6 (2σ, n = 45), corresponding to JMC-145 $^{176}Hf/^{177}Hf$ = 0.282163.

We determined oxygen isotopes using CO_2-laser fluorination and a Newwave 35W CO_2 laser at the University of Oregon (e.g. Bindeman, 2008). Single and bulk phenocryst grains and bulk groundmass weighing 0.6 to 2 mg were reacted with BrF_5 to release oxygen gas, which was

then purified in the laser chamber by several cryogenic traps (at liquid nitrogen temperature). Possible traces of fluorine gas were eliminated with a mercury diffusion pump. To react oxygen to CO_2, a small platinum graphite converter was employed. We analyzed the CO_2 gas on a MAT 253 mass spectrometer. For data quality control, several reference materials were included in each analytical run: four to seven aliquots of internal garnet standard, UOG1, $\delta^{18}O$ = 6.56‰, corresponding to the Gore Mt. Garnet ($\delta^{18}O_{olivine}$ = 5.8‰ VSMOW, Valley et al., 1995), and a San Carlos olivine with $\delta^{18}O_{olivine}$ = 5.25‰. Repeated $\delta^{18}O_{olivine}$ analyses basis were 0.1 to 0.25‰ less than the standards' accepted values, so the sample values were reduced accordingly. Replicate measurements of single grains and bulk groundmass do not exceed 0.15‰ (1σ) with one exception.

4. Results and descriptive comparison with the TSVZ

We provide new Sr-Nd-Pb isotope data for 37 basaltic to andesitic samples and Hf isotope data for 20 samples (Table 1). Seventeen mineral and groundmass samples were analyzed for O isotopes (Table 2). Major and trace element and volatile analyses for the samples for which we present isotope data in this study are published in Wehrmann et al. (2014) and in Wehrmann et al. (in rev), complemented by our new results for two VA samples CL 166 (Villarrica) and CL 701 (Casablanca), and the BA samples. These data are summarized in Supplementary Table 1 for the 37 samples in this study.

4.1 Major elements

Our CSVZ VA samples range from basalts to basaltic andesites to basaltic trachyandesites (SiO_2 = 49-61 wt. %) (Figure 2a), and most have 4-7 wt. % MgO, as compared to the TSVZ VA samples with 3-6 wt. % MgO, with one sample from the Los Hornitos cinder cones having 8.5 wt. % MgO (Jacques et al., 2013). The two trachyandesites from Lonquimay are the most evolved. All CSVZ samples plot in the medium-K and tholeiitic fields of Gill (1981). The CSVZ VA samples extend to lower K_2O at a given SiO_2 compared to the TSVZ samples (Figure 2b). The monogenetic cinder cone samples are basalts, except for one basaltic andesite from Apagado, and are characterized by lower SiO_2 (50-52 wt. %) and higher MgO contents (5.6-7.2 wt. %), forming the least differentiated end of the CSVZ trends in Figure 3. Otherwise there is substantial overlap between the CSVZ and TSVZ in major elements, especially at MgO > 4 wt. % (Figure 3). The BA samples are alkali basalts to trachybasalts, with SiO_2 = 47-56 wt. % and MgO = 2-9 wt. % (Figure 2a). Relative to the VA samples, the BA samples are in general shifted to lower SiO_2 but higher TiO_2, Na_2O, K_2O and P_2O_5 content at a given MgO content (Figure 3).

4.2 Trace elements

CSVZ VA samples show a pronounced subduction zone trace element signature on a multi-element diagram (Figure 4): characterized by enrichment relative to Rare Earth Elements (REE) in the fluid-mobile Large Ion Lithophile Elements (LILEs), such as Cs, Rb, K, Ba, U, Pb and Sr, by relative depletion in the High Field Strength Elements (HFSEs) Nb and Ta compared to fluid mobile elements, and by enrichment in melt-mobile elements such as Light (L) REE and Th relative to the Heavy (H) REE (Wehrmann et al., 2014). Whereas the fluid mobile and HRE

elements are similar or slightly enriched in the stratovolcanoes compared to the cinder cones, the HFSE and LREE are more depleted. Consequently, the stratovolcano samples have greater more to less fluid-mobile trace element ratios (e.g. Ba/Nb, U/Th, Pb/Ce) and lower more- to less-incompatible trace element ratios (e.g. Nb/Yb, La/Yb, La/Sm) than the cinder cone samples (e.g. Figure 4, 5 and 6). The basaltic andesite from the Apagado cinder cone is least enriched in incompatible elements, except Nb, K, Sr and Ti, it has a relative Ti peak compared to all other CSVZ samples with Ti troughs (Figure 4), and it has significantly lower La/Yb and higher U/Th than the other cinder cone samples (Figure 5). Our data are similar to previously published trace element data from Gerlach et al. (1988) and Hickey-Vargas et al. (1989) except for the higher Nb/Yb ratios they present for some monogenetic samples (Figure 6). The BA basalts are characterized by greater enrichment in most incompatible elements between Cs and Y with the exception of Pb and have lower contents of the heaviest HREE (Tm, Yb and Lu) (Figure 4b). Also the HREE of the BA rocks have a steeper negative slope. The BA basalts with the most enriched isotope ratios (MEBA) have the least arc-like enrichment in Th and Pb and lie on the MORB (Mid-Ocean Ridge Basalt)-OIB (Oceanic Island Basalt) array of Pearce (2008) on the Nb/Yb versus Th/Yb (Figure 6) and La/Yb ratios and have the highest, most MORB and OIB-like Nb/U and Ce/Pb (Hofmann et al., 1986) of the CSVZ BA samples (Figure 7). Nb/Yb, Th/Yb, Nb/U and Ce/Pb ratios overlap the BA basalts of the southernmost TSVZ (Jacques et al., 2013) and are similar to previously published compositions of SVZ BA basalts (Stern et al., 1990). The CSVZ MEBA basalts and the TSVZ southern BA basalts do not display Th and LREE enrichments. Compared to the TSVZ, the CSVZ stratovolcanoes have lower contents of all incompatible elements between Rb and Pb but higher HREE and Y abundances (Figure 4c). All samples closely follow the trench sediment pattern.

4.3 Isotopes

The CSVZ VA samples define a steep inverse correlation between $^{87}Sr/^{86}Sr$ and $^{143}Nd/^{144}Nd$ (Figure 8), with those from Llaima and Villarrica having the highest $^{143}Nd/^{144}Nd$ and the most offset to higher $^{87}Sr/^{86}Sr$ relative to $^{143}Nd/^{144}Nd$. The CSVZ stratovolcano samples are offset to higher $^{87}Sr/^{86}Sr$ at a given $^{143}Nd/^{144}Nd$ compared to the cinder cone samples, with no overlap between the two types of volcanic edifices. Our Sr and Nd isotope data are similar to those in previous studies (e.g. Harmon et al., 1984, Hickey et al., 1986, Hickey-Vargas et al., 1989, Gerlach et al., 1988, Sigmarsson et al., 1990). The Apagado cinder cone basaltic andesite, with significantly lower abundances of most incompatible elements compared to the other CSVZ samples, also has the most depleted Sr and Nd isotopic composition. All VA samples fall in the high $^{87}Sr/^{86}Sr$ half of the South Atlantic MORB field. The BA samples are shifted to lower Sr and Nd isotope ratios relative to the stratovolcano samples but most overlap the cinder cone and TSVZ samples. The five MEBA samples are shifted to higher $^{87}Sr/^{86}Sr$ and lower $^{143}Nd/^{144}Nd$ than all but one of the other BA samples.

On Pb isotope correlation diagrams (Figure 9), most CSVZ cinder cone samples overlap the TSVZ and CSVZ, but two samples extend to significantly less radiogenic ratios. As with Sr and Nd isotope ratios, the Apagado sample has the least radiogenic Pb isotope ratios. All but the Apagado sample plot in the lower part of the Chilean trench sediment field. The cinder cone array has a steeper slope than the stratovolcano array with the Apagado sample plotting well beneath the BA array on the thorogenic Pb isotope diagram (Figure 9). Excluding the MEBA samples, the other CSVZ and TSVZ BA samples overlap the CSVZ and TSVZ VA's and extend to less radiogenic Pb isotope ratios. The CSVZ BA samples, however, do not extend to such

unradiogenic Pb isotopic compositions as the TSVZ BA samples. The MEBA samples have distinctly higher $^{207}Pb/^{204}Pb$ and $^{208}Pb/^{204}Pb$ at a given $^{206}Pb/^{204}Pb$ (i.e. higher Δ7/4Pb and Δ8/4Pb) than the other CSVZ and TSVA BA samples.

On the εNd versus εHf isotope diagram, the stratovolcano and cinder cone samples overlap almost completely (Figure 10), in contrast to the Sr versus Nd isotope diagram. Two of the cinder cone samples also have less radiogenic compositions, just as is the case on the Pb isotope plots. The CSVZ VA samples extend to the highest ratios of all SVZ samples. The BA samples are displaced to lower Hf isotope ratios than the VA trend, as is also the case for the TSVZ BA relative to BAsamples (Jacques et al., 2013). The CSVZ MEBA samples extend the BA array to significantly lower Nd and Hf isotope ratios.

Oxygen isotopes ($\delta^{18}O$) from olivine and plagioclase (converted to $\delta^{18}O_{ol}$ by adding -0.7) phenocrysts from the CSVZ VA have $\delta^{18}O_{ol}$ values ranging from 4.53‰ to 5.50‰ (Table 2), slightly lower than for the TSVZ VA ($\delta^{18}O_{ol}$ = 4.88-5.62‰; Jacques et al., 2013), which extend well below to slightly above the mantle range for olivine (5.2‰ ± 0.2 or 5.0-5.4‰ Mattey et al., 1994). Samples from the CSVZ BA have $\delta^{18}O_{ol}$ ranging from 5.17‰ to 5.72‰. The $\delta^{18}O_{ol}$ for MORB glasses ranges from 5.5-5.9‰ (5.7 ± 0.2 ‰; Bindeman, 2008). If we convert $\delta^{18}O_{ol}$ to $\delta^{18}O_{melt}$ by adding a factor of 0.6 to the $\delta^{18}O_{ol}$ values, the range for the CSVZ and TSVZ $\delta^{18}O_{melt}$ is 5.13 to 6.32‰ (Table 2). We also measured $\delta^{18}O$ in glass/groundmass (representing the melt composition) from some of the same CSVZ and TSVZ samples (Table 2). The $\delta^{18}O$ in the glass/groundmass samples ranged from 5.37‰ to 6.35‰ (excluding BA sample CL 424), which is in good agreement with the $\delta^{18}O_{ol}$ converted to $\delta^{18}O_{melt}$. Comparing $\delta^{18}O$ in glass/groundmass with $\delta^{18}O_{melt}$ for individual samples, the difference is in most cases < 0.2 (Table 2), which is within the errors for the two measurements. The $\delta^{18}O_{glass/groundmass}$ and $\delta^{18}O_{melt}$ for sample CL 725

from Tinguiririca in the TSVZ VA show an exceptionally large discrepancy of 0.7. A second sample from the same sequence at Tinguiririca (CL 726), however, yielded an average $\delta^{18}O_{glass/groundmass}$ of 6.20 and $\delta^{18}O_{melt}$ of 6.22 very similar to the $\delta^{18}O_{glass/groundmass}$ of 6.31 for CL 725, suggesting that the olivine in sample CL 725 may not have been in equilibrium with the melt. Inspection of samples CL 032 and CL 424 suggest that the slightly higher $\delta^{18}O_{glass/groundmass}$ reflects hydration of these samples. This simple approach is more appropriate for our samples than using the linear equation from Bindeman et al. (2004), which calculates the Δ(min.-melt) based on the SiO_2 content of the whole rock and an assumed liquid line of descent in Kamchatka magmas. The Kamchatka equation probably overestimates the $\delta^{18}O_{melt}$ because the liquid line of descent of Andean magmas may be different. Since we have more $\delta^{18}O_{melt}$ data, we will show these data in figure 11 and only discuss this data henceforth.

The $\delta^{18}O_{melt}$ in the CSVZ stratovolcano samples overlap the lower end of the mantle range and extend to lower values, whereas the VA cinder cone samples overlap the mantle range and extend to slightly higher values (Figure 11). The VA cinder cone samples are within the TSVZ VA range (5.5-6.2‰; Table 2) and the Island arc range (5.5-6.8‰; e.g. Ewart et al., 1987, Turner et al., 2009, Vallier et al., 1991, Wade et al., 2005). $\delta^{18}O_{melt}$ of our CSVZ and TSVZ VA samples form crude inverse correlations with Nd isotopes, U/Th, Ba/Nb and Pb/Ce, and positive correlations with La/Yb (Figure 11). The stratovolcano samples have the highest highly fluid-mobile to less fluid-mobile trace element ratios and the lowest $\delta^{18}O_{melt}$, whereas the monogenetic CSVZ VA centers and TSVZ VA show the opposite. The $\delta^{18}O_{melt}$ of the CSVZ BA samples plot within the MORB range, except CL 424.

5. Discussion

We will first evaluate the evidence for crustal assimilation. Then, to identify the slab component and mantle wedge composition, we will discuss differences between the CSVZ VA stratovolcanoes versus CSVZ VA cinder cones and the TSVZ VA (using data from Jacques et al., 2013) and differences between the CSVZ and TSVZ BA samples. We will end with a quantitative flux melting model for generating the CSVZ melts.

5.1 Is crustal assimilation occurring during fractional crystallization in the CSVZ VA?

Crustal assimilation is possible throughout the SVZ VA because crustal thicknesses vary from 60 km to 40 km decreasing from north to south (e.g. Cembrano and Lara, 2009). The crust beneath the TSVZ VA diminishes towards the south and then remains at ~40 km beneath the CSVZ VA. If crustal assimilation occurred, a clear correlation between geochemical indicators for magma differentiation and isotopic compositions would be expected. Our isotope data, however, are not consistent with significant assimilation of isotopically contrasting crust during differentiation in either the TSVZ or CSVZ. As shown in figure 12, there is no substantial isotopic variation with decreasing MgO to 3 wt. % (or increasing SiO_2) in specific CSVZ volcanoes where there is enough data. The same lack of correlation is true for all differentiation indices (not shown). Osorno may be an exception but the difference in Nd isotopes is in only one sample from a different study and is not accompanied by a difference in Sr isotopes.

The Paleozoic and Mesozoic basement rocks, especially the Paleozoic ones, are characterized by higher $^{87}Sr/^{86}Sr$, higher $^{207}Pb/^{204}Pb$ and $^{208}Pb/^{204}Pb$ ratios at a given $^{206}Pb/^{204}Pb$ ratio, and lower $^{143}Nd/^{144}Nd$ than in the volcanic rocks (e.g. Figure 9; see also Lucassen et al.,

2004). On the uranogenic Pb isotope diagram, the TSVZ and the CSVZ VA samples form positive arrays below the crustal rocks. These arrays do not trend towards the crustal rocks but are subparallel to the bottom of the Mesozoic and Paleozoic crustal fields. The CSVZ cinder cones and TSVZ VA samples largely overlap in all isotopes, and the isotopic differences between the CSVZ and TSVZ stratovolcanoes cannot be explained by more assimilation of Paleozoic and Mesozoic basement in the TSVZ rocks.

The $\delta^{18}O$ of olivine converted to melt $\delta^{18}O$ ($\delta^{18}O_{melt}$) shows a restricted range for the CSVZ VA (5.13-6.10‰), which straddles the mantle range of 5.7 ± 0.2‰ (Bindeman, 2008), extending to slightly higher and lower values (Figure 11). $\delta^{18}O$ in arc rocks can deviate from the MORB mantle values of the mantle wedge through contributions from the subducting ocean crust (altered at low and high temperature) and sediments. Sediments generally have elevated $\delta^{18}O$, whereas the low-temperature-altered upper oceanic crust has high values and the hydrothermally-altered lower crust has low $\delta^{18}O$ (e.g. Bindeman et al., 2005, and references therein, Eiler et al., 2005, Jacques et al., 2013). The arc melts can also assimilate crust during ascent. Continental crust generally has high $\delta^{18}O$; however, hydrothermally-altered crustal rocks, such as older arc plutonic rocks, can have low $\delta^{18}O$ (see Bindeman et al., 2004, Bindeman, 2008, and references therein). Two samples from Minchinmávida-Chaitén have $\delta^{18}O_{melt}$ of 6.1 slightly higher than the mantle range. These samples also have the lowest Nd isotope ratios, which could reflect small amounts of crustal assimilation. These samples, however, plot on the CSVZ VA array on the uranogenic Pb isotope diagram and do not have elevated $^{207}Pb/^{204}Pb$ isotope ratios compared to the other CSVZ samples. Therefore any crustal assimilation would be minimal. The slightly elevated $\delta^{18}O_{melt}$ could also simply reflect addition of sediments into the subarc mantle, as has been proposed for TSVZ basalts (Jacques et al., 2013). Indeed, the $\delta^{18}O_{melt}$ in the

Minchinmávida-Chaitén samples are within the Island arc range of 5.5-6.8‰ (e.g. Ewart et al., 1987, Turner et al., 2009, Vallier et al., 1991, Wade et al., 2005). Assimilation of hydrothermally-altered plutonic roots could lower the $\delta^{18}O$ of VA melts, but this would require all CSVZ stratovolcanoes to have assimilated significant amounts of exclusively hydrothermally-altered plutonics. We believe this is unlikely considering the wide range in $\delta^{18}O$ of the plutonic rocks (-1.73‰ to 6.29‰; G. Jacques unpublished data) that we analyzed with values both substantially lower and higher than mantle rocks. We argue below that these differences reflect subcrustal processes that occur in the mantle and come from the slab. All of the CSVZ BA samples have $\delta^{18}O_{melt}$ within the error of the mantle range except sample CL 424 with elevated $\delta^{18}O_{melt}$ of 6.32‰. The elevated $\delta^{18}O$ could reflect crustal assimilation, which could also explain why this sample has the highest $^{207}Pb/^{204}Pb$ isotope ratio of all SVZ samples (Figure 9) and is shifted towards the field for Mesozoic and Paleozoic crust. This sample also has the lowest Nb/U of the MEBA samples and low Ce/Pb. Nevertheless, two other MEBA samples (CL 432 and CL 437) have mantle-like $\delta^{18}O$ favoring a mantle origin for the distinct isotopic enrichment of the MEBA samples.

The Miocene and younger intrusive rocks, which lie beneath the CSVZ volcanoes, have similar Sr-Nd-Pb isotopes to the Quaternary volcanic rocks (Table 1) (e.g. Figure 9; see also Lucassen et al., 2004). Assimilation of these crustal rocks would not significantly affect the radiogenic isotopes. Indeed, Jicha et al. (2007) and Reubi et al. (2011) proposed that the young plutonic roots of the CSVZ arc are variably assimilated at Puyehue and Llaima, respectively, based on U-series disequilibria. However, by their arguments, differentiation increases U-series disequilibria at Puyehue (Jicha et al., 2007) but decreases it at Llaima (Reubi et al., 2011), which makes it difficult to use differentiation to monitor assimilation. Assimilation of plutonic roots

also has been inferred at Tatara-San Pedro volcano in the TSVZ (Dungan et al., 2001; Dungan and Davidson, 2004) and at Mocho-Choshuenco (McMillan et al., 1989). Reubi et al. (2011) and McMillan et al. (1989) argued that such assimilation affects the most incompatible trace elements, such as Rb, Ba, U and Th, but not the isotopes because the magmas assimilate young crust with similar isotopic compositions. However, there is no evidence for enrichment in U or Th in the Tatara-San Pedro samples from Jacques et al. (2013) and there is no correlation between U/Th or Ba/Th and MgO or SiO_2 in our CSVZ samples (U/Th versus SiO_2 and versus Mg number: see Wehrmann et al., 2014). Dungan et al. (2001) and Dungan and Davidson (2004) used Rb/SiO_2 ratios to monitor assimilation in Tatara-San Pedro. There is no clear correlation between Rb/SiO_2 and isotope ratios in our samples (not shown).

In summary, although minor crustal assimilation may have occurred in a few of our samples, the differences in trace elements and isotopes between 1) the monogenetic cinder cones and the stratovolcanoes, and 2) the CSVZ and the TSVZ VAs cannot be explained by assimilation of older crust with different Sr-Nd-Pb isotopes and do not show clear evidence of assimilation of young intrusive rocks with similar Sr-Nd-Pb isotopes. We attribute this lack of assimilation to reuse of conduits that became insulated from the crust by freezing of earlier melts on sidewalls. Moreover, south of 37°S, the volcanoes are located on tension cracks and large intra-arc fault systems that reach the surface (e.g. the Liquine-Ofqui Fault Zone) and allow magmas to ascend easily and quickly (Cembrano and Lara, 2009). Below we discuss subcrustal processes that can explain the geochemical differences we observe.

5.2 CSVZ VA stratovolcanoes compared to CSVZ VA cinder cones and TSVZ VA: Differences in the mass fraction of the slab component

The CSVZ VA stratovolcano and monogenetic cinder cone samples show systematic differences in geochemistry with the cinder cones often overlapping the TSVZ VA samples. Compared to the CSVZ VA cinder cone and the TSVZ VA samples, the CSVZ VA stratovolcano samples have higher ratios of highly fluid-mobile to less fluid-mobile trace elements (e.g. U/Th, U/Nb and Pb/Ce), reflecting a larger mass fraction of slab fluid in the source of the CSVZ stratovoclanoes, and lower ratios of more-incompatible to less-incompatible trace elements (e.g. La/Yb. Nb/Yb), reflecting higher degrees of melting and/or derivation from more depleted source material (e.g. Figure 5, 6 and 7). The more radiogenic Pb isotopic compositions of the CSVZ stratovolcanoes, plotting completely in the field for trench sediments, are also consistent with a greater addition of slab component to the mantle source. The simplest explanation for these combined differences is that a higher flux of fluids from the slab (altered ocean crust (AOC) and sediment) beneath the CSVZ stratovolcanoes caused greater amounts of flux melting. Greater amounts of melting resulted in greater volumes of magma being produced that formed larger volcanic edifices (stratovolcanoes compared to monogenetic vents). Hickey-Vargas et al. (1989, 2002 and references therein) reached a similar conclusion for Villarrica and its surrounding monogenetic cones and rear-arc centers (Quetrupillán and Lanín).

Our phenocryst-based data for CSVZ stratovolcano samples have lower $\delta^{18}O_{melt}$ than the MORB range (5.5-5.9‰, Bindeman (2008) and references therein), whereas the CSVZ cinder cone and TSVZ samples overlap the MORB range or extend to slightly higher values (Figure 11). The trench sediments in Chile have high $\delta^{18}O$ (8-14‰, Jacques et al., 2013). Therefore the slightly elevated $\delta^{18}O$ in the CSVZ cinder cone and TSVZ samples could reflect the addition of sediment to their mantle wedge source. In order to explain the lower values found in the CSVZ

stratovolcano samples, a component with low $\delta^{18}O$ (e.g. serpentine, 0-6‰, Bindeman et al., 2005 and references therein) is needed to compensate the high $\delta^{18}O$ in the sediments. Samples having the highest εHf and εNd isotopes have the lowest $\delta^{18}O_{melt}$ (Figure 10, 11), consistent with derivation of low $\delta^{18}O$ fluids from a depleted reservoir such as hydrothermally-altered lower oceanic crust and/or serpentinized upper mantle of the incoming slab (Figure 11). A similar observation in Central America led Eiler et al. (2005) and Heydolph et al. (2012) to propose that fluids from serpentinites or altered gabbros in the lower crust were the cause of the lower than typical mantle $\delta^{18}O$ in olivine.

5.3 Differences in the composition of the mantle wedge, subducting oceanic crust, and subducting sediment

5.3.1 The mantle wedge

The CSVZ VA samples have lower ratios of highly incompatible to less incompatible trace elements (e.g. Nb/Yb, La/Yb, Th/Yb; Figure 5 and 6) than the TSVZ VA samples. Some literature data from the rear-arc volcanoes Lanín and Quetrupillán overlap our TSVZ data, but most samples from Villarrica, Llaima and Puyehue volcanoes and nearby monogenetic cones overlap our CSVZ VA samples (Gerlach et al., 1988; Hickey-Vargas et al., 1989). The lower Nb/Yb indicates a more depleted mantle wedge and/or higher degree of melting beneath the CSVZ VA. Although the range of εNd and εHf is small within the CSVZ (e.g., 2 εNd units; Figure 10), there is a rough negative correlation with Nb/Yb for the CSVZ stratovolcanoes that define the depleted end of an array that includes the entire SVZ VA (not shown). Therefore, the

variations in trace element ratios reflect differences in source composition and not just in the degree of mantle melting. Because Hf is the least likely isotopic tracer to be modified by a slab-derived component, we conclude that the mantle wedge beneath the CSVZ VA is more depleted (more N-MORB-like) than beneath the TSVZ VA segment (more E-MORB-like or reflects a mixture between MORB and ocean-island basalt type component).

In the TSVZ, Jacques et al. (2013) concluded that the mantle wedge beneath the arc can be best represented by two end-members: depleted South Atlantic mantle (SAM-D with lower Sr and Pb and higher Nd isotope ratios), and enriched South Atlantic mantle (SAM-E with slightly higher Sr and Pb and lower Nd isotope ratios). These end-members were constrained using BA basalts largely free of slab influence, but Hf isotope ratios in the TSVZ BA are systematically lower relative to Nd isotopes than in the VA. The same traits also characterize the CSVZ. We conclude that the mantle wedge beneath the CSVZ VA is also heterogeneous isotopically and similar to the TSVZ VA, despite being primarily more depleted in the most incompatible trace elements.

Most CSVZ BA basalts overlap the TSVZ BA basalts on all isotope plots (Figure 8, 9, 10). Five CSVZ MEBA samples have more enriched isotopic compositions than the other BA samples, having more radiogenic $^{87}Sr/^{86}Sr$ and $^{207}Pb/^{204}Pb$ and $^{208}Pb/^{204}Pb$ at a given $^{206}Pb/^{204}Pb$, but less radiogenic $^{143}Nd/^{144}Nd$ and $^{176}Hf/^{177}Hf$. As noted above, sample CL 424 with elevated $\delta^{18}O$, the highest $^{207}Pb/^{204}Pb$ isotope ratio of all SVZ samples, the lowest Nb/U of the MEBA samples and low Ce/Pb may have assimilated some crust. The mantle-like $\delta^{18}O$ in two other MEBA samples favor a mantle origin for the distinct isotopic enrichment of the MEBA samples with less radiogenic Pb. The MEBA samples also have less pronounced Nb-Ta troughs and thus higher Nb/U ratios (within the typical mantle range of 47 ± 10 as defined by Hofmann et al.,

1986; Figure 7) and less pronounced Pb peaks and thus higher Ce/Pb and Nd/Pb ratios than most of the other CSVZ BA samples, reflecting less of a slab-derived component in these samples (Figure 7). The CSVZ MEBA samples and the southernmost TSVZ BA samples are free from slab-derived Th and LREE (Figure 6), but they differ isotopically. Both CSVZ MEBA and TSVZ BA samples have similar Sr, Nd and O isotopes to the "cratonic" basalts of Stern et al. (1990), who proposed that they were formed by small degree partial melting of heterogeneous subcontinental lithosphere and/or asthenosphere, without influence from slab-derived fluids. The BA and MEBA compositions could reflect the involvement of two distinct types of enriched subcontinental lithosphere, either located in the lithosphere or as delaminated enriched plums in the asthenospheric mantle (Kay et al., 2013). A contribution from enriched subcontinental lithospheric mantle in the BA could potentially explain why the BA and MEBA volcanic rocks, in contrast to the VA rocks, plot below the South Atlantic MORB field on the Nd versus Hf isotope diagram (Figure 10). Thus the mantle wedge asthenosphere may have a South Atlantic MORB type composition in the absence of lithospheric components. Enriched lithospheric components could be largely melted out of the asthenospheric wedge mantle in the backarc. Enriched lithospheric plums in the mantle wedge beneath the VA would be largely swamped by greater degrees of flux melting beneath the arc.

5.3.2 Subducting altered oceanic crust (AOC)

The oceanic crust currently subducting beneath both the TSVZ and CSVZ probably formed at the EPR. However, the age of subducting crust is ambiguous south of the Valdivia

fracture zone and might have formed at the Chile Ridge (Herron et al., 1981; Tebbens and Cande, 1997; Tebbens et al., 1997).

MORB forming now at the northern Chile Ridge is similar to EPR MORB but with higher Δ7/4Pb (Bach et al., 1996). However, crust of this type is not yet subducting. In contrast, MORB forming now at the southern Chile Ridge is isotopically enriched (Klein and Karsten, 1995; Sturm et al., 1999), is part of the global DUPAL anomaly, and is similar to Southern Atlantic enriched mantle (SAM-E). It may reflect flow of such mantle through the slab window associated with the subduction of the Chile Ridge. This enriched crust may be subducting beneath the southernmost part of the CSVZ, i.e. Apagado and Chaitén.

Subduction of isotopically enriched AOC, however, cannot explain the differences between the TSVZ and CSVZ, because the CSVZ is characterized by more depleted Nd isotopes, rather than more enriched. Indeed, the southernmost CSVZ volcanoes, beneath which enriched AOC is most likely to be subducting, are characterized by the most depleted isotopes (i.e. Apagado).

5.3.3 Subducting sediment

The trench sediments are generally similar in composition along strike, but there is a slight increase in average $^{87}Sr/^{86}Sr$ and Ce/Pb, and decrease in average $^{143}Nd/^{144}Nd$ and Ba/La southward due to more continent-derived material supplied by greater erosion in this region of the Andes (Lucassen et al., 2010; Plank, 2011). Although the $^{87}Sr/^{86}Sr$ ratio of the CSVZ stratovolcanoes is slightly higher than in the TSVZ, the Ce/Pb ratio is similar and the $^{143}Nd/^{144}Nd$ and Ba/La ratios are higher, not lower as observed in the sediments in the south. Moreover, a

difference in sediment composition cannot explain the shift to lower $\delta^{18}O_{melt}$ of the CSVZ samples compared to the TSVZ samples, because the trench sediments have high $\delta^{18}O$ (Jacques et al., 2013).

5.4 Difference in slab surface temperature beneath the Volcanic Front

The slab surface beneath the CSVZ should be slightly hotter than beneath the TSVZ because the slab is younger to the south yet the depth to the slab beneath the VA is similar (van Keken et al., 2011). A hotter slab would be more likely to melt, and melts could more readily transport fluid-immobile elements such as Nb, Ta, Hf and Zr. However, the CSVZ samples have lower ratios of these elements to HREE (e.g. Figure 6) than in the TSVZ, which can indicate higher degrees of mantle melting, greater source depletion through melt extraction or a lower slab-melt flux. The inverse correlation of Nb/Yb with Nd isotopes, mentioned above, suggests that differences in degree of melting alone do not govern the variations in HFSE/HREE ratios. The numerical model presented in Section 5.6 evaluated the effects of different slab surface temperatures and found them to be insignificant. Therefore, the difference in slab surface temperature does not explain the differences between the TSVZ and CSVZ.

5.5 Differences in the amount of slab serpentinization

There are numerous fracture zones, including the large Valdivia and Chiloé fracture zones, on the incoming Nazca Plate outboard of the CSVZ (Figure 1). The Valdivia fracture zone, if projected beneath the CSVZ in the direction of plate motion, would be located beneath

Villarrica (believed to be one of South America's most active volcanoes) at ~39°S (Dzierma et al., 2012a). The Chiloé fracture zone may arrive beneath Puyehue. A similar cluster of seismic events between the slab and the Earth's surface is present beneath both Villarrica and Puyehue (Dzierma et al., 2012a,b). There are also numerous bend-faults on the outer rise of the Nazca Plate, although largely buried by sediments outboard of the CSVZ (Ranero et al., 2005; Ranero et al., 2006, Contreras-Reyes et al., 2007). These fracture zones and bend-faults provide pathways for water to enter and hydrothermally alter the lower crust and to serpentinize the upper mantle (e.g. Ranero et al., 2003; Rüpke et al., 2002, 2004; Grevemeyer et al., 2007; Contreras Reyes et al., 2007). The abundance and extent of both fracture zones and bend-faults (which can be identified west of the trench in Figure 1 despite the sediment cover) are greater outboard of the CSVZ than the TSVZ and therefore it is likely that the plate outboard of the CSVZ has been more extensively hydrated (Dzierma et al., 2012a). As a consequence of the greater hydration, larger amounts of water are available for being released and added to the mantle wedge beneath the CSVZ compared to the TSVZ.

Local earthquake tomography shows a low velocity anomaly and high Vp/Vs values beneath the CSVZ forearc between 39°-40°S (Dzierma et al., 2012a). These features are consistent with serpentinization and/or underthrusting of forearc material such as sediments. The same velocity anomaly and Vp/Vs values were observed along the projected Valdivia fracture zone further east, extending from the slab to the crust beneath the VA at Villarrica. These observations are evidence of high fluid flux at Villarrica in particular, and other CSVZ stratovolcanoes in general, and it seems likely to be related to the subduction of more fracture zones and bend-faults beneath the CSVZ than the TSVZ.

In summary, based on geophysical, morphological and geochemical data, we attribute the differences between the TSVZ versus CSVZ VA to higher slab-derived fluid flux in the CSVZ that coincides with the presence of large fractures zones and more extensive bend-faulting on the incoming plate that can hydrate the subducting lower crust and underlying upper mantle. Highly serpentinized mafic and ultramafic portions of the slab may form a larger water reservoir that can be released to the mantle wedge beneath the volcanic front resulting in higher degrees of mantle melting. The higher magma flux, higher ratios of fluid-mobile to other trace elements and higher $^{87}Sr/^{86}Sr$, $^{143}Nd/^{144}Nd$ and $^{177}Hf/^{176}Hf$ ratios in the CSVZ relative to the TSVZ are consistent with this simple tectonic difference along strike of the incoming plate outboard the arc.

5.6 Quantitative flux melting model

We quantified our arguments by using the Arc Basalt Simulator version 3.10 of Kimura et al. (2009, 2010). This approach was successfully applied to the TSVZ segment (Jacques et al., 2013) to which we make comparison. The model predicts that TSVZ basalts are produced by a slab melt derived from 60 % trench sediments and 40 % AOC. Addition of a few percent of this slab component to an enriched heterogeneous mantle wedge causes ca. 1 % melting of the mantle.

We assumed the same sediment composition (sample 75Kd(1) from Lucassen et al., 2010; Table 3) for the CSVZ as for the TSVZ, because this sample was taken offshore of the CSVZ (Figure 1b). Its composition is close to the average marine sediment composition estimated by of Plank (2011) at 40°S, and it has the most radiogenic Pb. Choosing sediment with even more radiogenic Sr has little effect on our results. We also assumed the same AOC values

that are from the western Pacific (Kelley et al., 2003; Table 3), even though the AOC beneath the CSVZ is younger and probably less altered than for the TSVZ. Using southern Chile Ridge instead of EPR basalt for AOC does not affect our results, because 30% sediment swamps the AOC trace element composition.

For the mantle wedge, we again used the DMM trace element composition from Workman and Hart (2005) and the isotopic compositions of Jacques et al. (2013) (SAM-D and SAM-E) plus one in between (Table 3). We assume that these compositions represent the least slab-contaminated mantle wedge beneath the CSVZ. Even though we argued above that the mantle wedge beneath the CSVZ may be more depleted in trace elements than the TSVZ (Section 5.4.1), the model does not require more depleted DMM concentrations. Likewise, the model does not require mantle sources more enriched than SAM-E, such as found in the CSVZ backarc (MEBA samples). As discussed above, we infer that such components are melted out in the backarc prior to advection beneath the arc itself.

We modeled sample CL 170 from Villarrica which is our most mafic sample from the CSVZ with MgO = 7.4 wt. %. The most satisfactory results were obtained when adding a slab melt to DMM from a source that is 30 % sediment and 70 % AOC. We assumed formation of the slab component directly beneath the CSVZ stratovolcanoes (130 km; ~3.9 GPa) at the slab surface temperature calculated for the CSVZ by van Keken et al. (2011). We then adjusted the P-T conditions of mantle melting to best match the trace element pattern and isotopic composition of CL 170. The best match is obtained for mantle melting at 1.9 GPa and 1230°C. For trace element concentrations, the best match requires addition of 2 to 6 % slab component, whereas for isotopes less than 2 % slab component is needed. This inconsistency probably reflects limitations of ABS3.10 (e.g., the assumption that sediment and AOC melt equally, and the lack of a separate

AOC-derived fluid component), uncertainties in trace element partition coefficients, and the role of accessory phases. Adding <2 to 6 % slab component causes <1.6 to 5.5 % mantle melting under these conditions, and the resulting primitive basalts contain about 3-4 wt. % water. The amount of slab component added to the mantle beneath the CSVZ is slightly higher than beneath the TSVZ.

We also modeled the monogenetic cinder cones using samples CL 017 and CL 088 with MgO = 5-7 wt. %. The P-T conditions of mantle melting needed to match the trace elements differ from those for the stratovolcanoes. Mantle melting occurs at 1.9-2.0 GPa and 1270-1280°C, which is similar to the P-T conditions at the TSVZ VA (Jacques et al., 2013) but temperature is higher than for the CSVZ stratovolcanoes. For CL 017, only 1 % of slab component is needed to best match the trace element concentrations, while 3 % slab component is needed for CL 088. The degree of mantle melting under these conditions varies from 1 % to 3.5 %, and the resulting basalts contain ca. 2 wt. % water. This is consistent with their inferred lower degree of melting (e.g. higher La/Yb), lower amount of slab component (lower Sr and Nd isotope ratios), and smaller magma volumes than in the surrounding stratovolcanoes. However, matches for La, Ce, Sr, Zr and Hf, and to lesser extent, U and Y, are not as good as for the stratovolcanoes; the calculated basalts have lower concentrations than the targets. Nevertheless, the overall modelling is robust and supports the geochemical observations made in the previous sections.

Our quantitative model differs from our qualitative conclusions in one key respect. As for the TSVZ, the model includes only a water-saturated melt of both slab sediment and AOC; it does not include the additional fluid flux from the colder gabbroic and ultramafic portion of the slab that we infer for the CSVZ from its distinctively higher LILE/REE and lower $\delta^{18}O$ ratios.

This limitation reflects inherent features of the ABS3.10 code that are being modified in version ABS4, presently in review. However, the higher AOC:SED ratio for the slab component in our model for the CSVZ relative the TSVZ partly reflects the greater role of fluid from serpentinite and the lower oceanic crust in the CSVZ.

Figure 13 shows the modeling results for Sr-Nd and Sr-Pb isotopes. The central mixing line goes through the Llaima and Villarrica samples. The Osorno, Mocho-Choshuenco and Minchinmávida-Chaitén samples, which have higher Sr isotopes, and the Apagado sample, which is the most depleted, are bracketed by the mixing lines to the SAM-E and SAM-D mantle wedge components, respectively. The Apagado sample is the closest sample to the SAM-D component, which agrees with its depleted trace element and isotope ratios.

We will now compare our model results for the CSVZ to the results for the TSVZ using the same ABS3.10 modelling (Jacques et al., 2013). The AOC:SED ratio in the slab component differs between the TSVZ (40:60) and the CSVZ (70:30), and is the same for stratovolcanoes and cinder cones in the CSVZ. The mass fraction of slab component (inferred from isotopes), and the degrees of mantle melting, are different between the segments. The amount of slab component in the TSVZ VA and CSVZ cinder cones is less than 1 %, whereas the CSVZ stratovolcano samples require ca. 2 %. Our models also predict 1.0-1.2 % mantle melting at 2.1 GPa and 1270°C for the TSVZ stratovolcanoes, versus 1.6-5.5 % melting at 1.9 GPa and 1240°C for the CSVZ stratovolcanoes. This is consistent with the higher degrees of mantle melting beneath CSVZ stratovolcanoes inferred from their lower Nb/Yb and Th/Yb ratios assuming a homogeneous source (Figure 6).

The pressure and temperature of the slab surface beneath the CSVZ (3.9 GPa, 845°C) differs only slightly from the TSVZ (4 GPa, 830°C). The modal mineralogy of AOC and

sediment at these P-T conditions (van Keken et al., 2011) is relatively similar for both segments, but no phengite is left in the AOC beneath the CSVZ VA (Table 4), which increases trace element bulk partition coefficients and decreases Pb/Nd fractionation. This indicates that dehydration of the mafic part of the slab is more complete beneath the CSVZ VA even though the slab surface reaches higher P (but lower T) beneath the TSVZ. The ABS model predicts that most fluid is lost from the sediment and AOC beneath the CSVZ forearc, and thus serpentinite dehydration must be the primary source of fluid beneath the CSVZ VA.

The phase diagrams used by ABS for AOC and sediment (from Hermann and Spandler, 2008) predict 22 % water-saturated slab melting beneath the CSVZ versus 18 % in the TSVZ (Jacques et al., 2013). Our conclusion that both sediment and AOC melt beneath the CSVZ volcanic front is consistent with the thermal model of van Keken et al. (2011) in which the temperature in the top several km of the slab exceeds the water-saturated solidi of both sediment and basalt. The slightly higher degree of slab melting beneath the CSVZ might also be caused by more serpentine-derived fluid, which increases slab melting. Our model differs slightly from the conclusion of Watt et al. (2013) that slab melting only occurs behind the volcanic front at Apagado, but the small mass fraction of slab component that we infer for Apagado renders the distinction moot. The elevated Th/Yb ratios in all volcanic arc samples (Figure 6) are consistent with the slab component being a melt. Moreover, slab melting increases the potential to carry relatively fluid-immobile elements such as Nd and Hf. This, plus the higher % AOC in our CSVZ slab component, is consistent with the CSVZ stratovolcanoes having higher Nd and Hf isotope ratios compared to the TSVZ. The serpentine-derived fluid may be the source of excess U over Th observed in most CSVZ stratovolcanoes.

6. Conclusions

We used trace element and Sr-Nd-Hf-Pb-O isotope data to compare and contrast monogenetic cinder cones and stratovolcanoes within the CSVZ (38-43°S), the CSVZ VA and BA, and the CSVZ and the TSVZ VA (34.5-38°S) segments. The CSVZ BA is similar to that of the TSVZ but contains an additional enriched component in some areas, either in the lithosphere or in the asthenospheric mantle wedge. Compared to the CSVZ cinder cones and TSVZ, the CSVZ stratovolcanoes have greater highly fluid-mobile to less fluid-mobile trace element ratios (such as U/Th, Pb/Ce, Ba/Nb), lower incompatible to less incompatible trace element ratios (such as La/Yb), lower $\delta^{18}O_{melt}$, and higher Nd and Hf isotopes. The cinder cones differ from the stratovolcanoes by having less of a slab-derived component in their source resulting in smaller degrees of melting. The combined morphological, geophysical and geochemical data suggest an enhanced fluid flux beneath the CSVZ stratovolcanoes, as compared to the TSVZ volcanoes, resulting in greater magma production, reflected in increased eruption rates in the past and the present in the CSVZ.

No clear evidence for coupled assimilation, fractionation and crystallisation (AFC) processes was found in our samples, as was proposed by Jicha et al. (2007) and Reubi et al. (2011) for Puyehue and Llaima volcanoes, respectively. Our geochemical data indicate that the processes are subcrustal and come primarily from the slab. However, the along-strike variations are not related to changes in the subducting AOC or sediments.

Instead, we favor enrichment of the CSVZ mantle wedge by melts and fluids from the incoming Nazca plate. It is likely that the lower oceanic crust has been hydrothermally altered and the underlying upper mantle has been serpentinized due to the deep introduction of seawater

via large and abundant fracture zones and faults related to the bending of the plate outboard the trench. This scenario is in agreement with geophysical observations of a low velocity zone along fracture zones (Dzierma et al., 2012), which is interpreted to reflect more abundant serpentinite in the mantle wedge beneath the CSVZ forearc extending beneath Villarrica Volcano.

Our quantitative mass balance model supports our geochemical observations. Trace element patterns and Sr-Nd-Pb isotopes are best modeled by adding <2 to 6 % of a slab melt derived from a 30:70 SED:AOC source beneath the CSVZ VA versus 0.5-1 % of a slab melt from a 60:40 SED:AOC source beneath the TSVZ VA. Addition of the slab component causes 1.6-5.5 % melting of the mantle at about 1.9 GPa and 1240°C in the CSVZ versus 1.0-1.2 % mantle melting at 2.1 GPa and 1270°C for the TSVZ.

Acknowledgment

We thank F. and S. Hauff for their excellent support of the isotope facilities. We thank P. van den Bogaard from GEOMAR, as well as J. Clavero and SERNAGEOMIN for their support with the field studies. We are also grateful to two anonymous reviewers who helped to increase the quality of this article. This paper is contribution No. 268 of Collaborative Research Center (Sonderforschungsbereich) SFB574 “Volatiles and Fluids in subduction Zones” at Kiel University, funded by the German Research Foundation. JG’s contribution to this paper was supported by an Alexander von Humboldt Research Prize. IB acknowledges NSF grants EAR-0844772 and EAR-0948455.

References

Amante C. and Eakins B.W. (2009) ETOPO1 1 Arc-Minute Global Relief Model: Procedures, Data sources and Analysis, NOAA Technical Memorandum NESDIS NGDC-24, 19pp

Andres M., Blichert-Toft J. and Schilling J.G. (2002) Hafnium isotopes in basalts from the Southern Mid-Atlantic Ridge from 40° to 55°S: Discovery and Shona plume-Ridge interactions and the role of recycled sediments, *Geochem Geoph Geosy* **3**

Angermann D., Klotz J. and Reigber C. (1999) Space geodetic estimation of the Nazca-South America Euler vector, *Earth Planet Sci Lett* **171**, 329-334

Bach W., Erzinger J., Dosso L., Bollinger C., Bougault H., Etoubleau J. And Sauerwin J. (1996) Unusually large Nb-Ta depletions in North Chile Ridge basalts at 36°50' to 38°56'; major element, trace element and isotopic data, *Earth Planet Sci Lett* **142**, 223-240

Bindeman I.N., Ponomareva V.V., Bailey J.C. and Valley J.W. (2004) Volcanic arc of Kamchatka: a province with high-$\delta^{18}O$ magma sources and large scale $^{18}O/^{16}O$ depletion of the upper crust, *Geochim Cosmochim Ac* **68**, 841-865

Bindeman I.N., Eiler J.M., Yogodzinski G.M., Tatsumi Y., Stern C.R., Grove T.L., Portnyagin M., Hoernle K. and Danyushevsky L.V. (2005) Oxygen isotope evidence for slab melting in modern and ancient subduction zones, *Earth Planet Sci Lett* **235**, 480-496

Bindeman I.N. (2008) Oxygen isotopes in mantle and crustal magmas as revealed by single crystal analysis, *Rev Mineral Geochem* **69**, 445-478

Blichert-Toft J. and Albarède F. (1997) The Lu-Hf isotope geochemistry of chondrites and the evolution of the mantle-crust system, *Earth Planet Sci Lett* **148**, 243-258

Cembrano J. and Lara L.E. (2009) The link between volcanism and tectonics in the southern volcanic zone of the Chilean Andes: a review, *Tectonophysics* **471**, 96-123

Contreras-Reyes E., Grevemeyer I., Flueh E.R., Scherwath M. and Heesemann M. (2007) Alteration of the subducting oceanic lithosphere at the southern central Chile trench-outer rise, *Geochem Geoph Geosy* **8**

Contreras-Reyes E., Grevemeyer I., Flueh E.R. and Reichert C. (2008) Upper lithospheric structure of the subduction zone offshore of southern Arauco peninsula, Chile, at ~38°S, *J Geoph Res* **113**

Douglass J., Schilling J.G. and Fontignie D. (1999) Plume-ridge interactions of the Discovery and Shona mantle plumes with the Southern mid-Atlantic ridge (40-55 degree South), *J Geoph Res* **104**, 2941-2962

Dungan M.A., Wulff A. and Thompson R. (2001) Eruptive stratigraphy of the Tatara-San Pedro complex, 36°S, Southern Volcanic Zone, Chilean Andes: reconstruction method and implications for magma evolution at long-lived arc volcanic centers, *J Petrol* **42**, 555-626

Dungan M.A. and Davidson J.P. (2004) Partial assimilative recycling of the mafic plutonic roots of arc volcanoes: an example from the Chilean Andes, *Geology* **32**, 773-776

Dzierma Y., Rabbel W., Thorwart M., Koulakov I., Wehrmann H., Hoernle K. And Comte D. (2012a) Seismic velocity structure of the slab and continental plate in the region of the 1960 Valdivia (Chile) slip maximum – Insights into fluid release and plate coupling, *Earth Planet Sci Lett* **331-332C**, 164-176

Dzierma Y., Thorwart M., Rabbel W., Siegmund C., Comte D., Bataille K., Iglesia P. And Prezzi P. (2012b) Seismicity near the slip maximum of the 1960 Mw 9.5 Valdivia earthquake

(Chile): Plate interface lock and reactivation of the subducted Valdivia Fracture Zone, *J Geoph Res* **117**, 13pp

Elliot T., Plank T., Zindler A., White W. and Bourdon B. (1997) Element transport from slab to volcanic front at the Mariana arc, *J Geoph Res* **102**, 14991-15019

Eiler J.M., Carr M.J., Reagan M. and Stolper E. (2005) Oxygen isotope constraints on the source of Central American arc lavas, *Geochem Geoph Geosy* **6**

Ewart A. and Hawkesworth C.J. (1987) The Pleistocene-Recent Tonga-Kermadec arc lavas: Interpretation of new isotopic and Rare Earth data in terms of Depleted Mantle source model, *J Petrol* **28**, 495-530

Fontignie D. and Schilling J.G. (1991) $^{87}Sr/^{86}Sr$abd REE variations along the Easter microplate boundaries (South Pacific): application of multivariate statistical analyses to ridge segmentation, *Chem Geol* **89**, 209-241

Fontignie D. and Schilling J.G. (1996) Mantle heterogeneities beneath the South Atlantic: a Nd-Sr-Pb isotopes study along the mid-Atlantic ridge (3 degree South-46 degree South), *Earth Planet Sci Lett* **142**, 209-221

Futa K. and Stern C.R. (1988) Sr and Nd isotopic and trace element compositions of Quaternary volcanic centers of the Southern Andes, *Earth Planet Sci Lett* **88**, 253-262

Geldmacher J.R. and Hoernle K. (2006) Origin and geochemical evolution of the Madeira-Tore Rise (eastern North Atlantic), *J Geoph Res* **111**

Gerlach D., Frey F.A., Moreno H. And López-Escobar L. (1988) Recent volcanism in the Puyehue-Cordón Caulle region, southern Andes, Chile (40.5°S): Petrogenesis of evolved lavas, *J Petrol* **29**, 333-392

Gill J.B. (1981) Orogenic andesites and plate tectonics, Berlin, Heidelberg, New York, Tokyo, Springer, 390p

Green T.H., Blundy J.D., Adam J. and Yaxley G.M. (2000) SIMS determination of trace element partition coefficients between garnet, clinopyroxene, and hydrous basaltic liquids at 2-7.5 GPa and 1080-1200°C, *Lithos* **53**, 165-187

Grevemeyer I., Ranero C.R., Flueh E.R., Kläschen D. and Bialas J. (2007) Passive and active seismological study of bending-related faulting and mantle serpentinization at the Middle America trench, *Earth Planet Sci Lett* **258**, 528-542

Haase K.M. (2002) Geochemical constraints on magma sources and mixing processes in Easter microplate MORB (SE Pacific); A case study of plume-ridge interaction, *Chem Geol* **182**, 335-355

Hamelin B., Dupré B. and Allègre C.J. (1984) Lead-Strontium isotopic variations along the East Pacific Rise and the Mid-Atlantic Ridge: a comparative study, *Earth Planet Sci Lett* **67**, 340-350

Hanan B.B., Kingsley R.H. and Schilling J.G. (1986) Pb isotope evidence in the South Atlantic for migrating ridge-hot spots interactions, *Nature* **322**, 137-144

Hanan B.B. and Schilling J.G. (1989) Easter microplate evolution: Pb isotope evidence, *J Geoph Res* **94**, 7432-7448

Harmon R.S., Barreiro B.A., Moorbath S., Hoefs J., Francis P.W., Thorpe R.S., Deruelle B., McHugh J. and Viglino J.A. (1984) Regional O-, Sr-, and Pb-isotopes relationships in late Cenozoic calc-alkaline lavas of the Andean cordillera, *J Geol Soc London* **141,** 803

Hermann J. and Spandler C.J. (2008) Sediment melts at sub-arc depths: an experimental study, *J Petrol* **49**, 717-740

Herron E.M., Cande S.C. and Hall B.R. (1981) An active spreading center collides with a subduction zone – a geophysical survey of the Chile margin triple junction, *Geol Soc Am Mem* **154**, 683-701

Heydolph K., Hoernle K., Hauff F., van den Bogaard P., Portnyagin M., Bindeman I. and Garbe-Schönberg C.-D. (2012) Along- and across-arc geochemical variations in nortwestern Central America: Increased contribution of enriched lithosphere to lavas along the volcanic from Nicaragua to Guatemala and behind the volcanic front, *Geochim Cosmochim Ac* **84**, 459-491

Hickey R.L., Gerlach D.C. and Frey F.A. (1984) Geochemical variations in volcanic rocks from central-south Chile (33°-42°S). In: Harmon R.S. and Barreiro B.A. (eds) Andean Magmatism: Chemical and Isotopic Constraints. Shiva Publishing Limited, pp. 72-95, Nantwich, U.K.

Hickey R.L., Frey F.A. and Gerlach D.C. (1986) Multiple sources for basaltic arc rocks from the Southern Volcanic Zone of the Andes (34°-41°S): Trace element and isotopic evidence for contributions from subducted oceanic crust, mantle, and continental crust, *J Geoph Res* **91**, 5963-5983

Hickey-Vargas R.L., Moreno Roa H., Lopez-Escobar L. and Frey F.A. (1989) Geochemical variations in Andean basaltic and silicic lavas from the Villarrica-Lanin volcanic chain (39.5°S): an evaluation of source heterogeneity, fractional crystallization and crustal assimilation, *Contrib Mineral Petrol* **103**, 361-386

Hickey-Vargas R.L., Sun M., López-Escobar L., Moreno-Roa H., Reagan M.K., Morris J.D. and Ryan J.G. (2002) Multiple subduction components in the mantle wedge: Evidence from eruptive centers in the Central Southern Volcanic Zone, Chile, *Geology* **30**, 199-202

Hildreth W. and Moorbath S. (1988) Crustal contributions to arc magmatism in the Andes of Central Chile, *Contrib Mineral Petrol* **98**, 455-489

Hoernle K., Abt D.L., Fisher K.M., Nichols H., Hauff F., Abers G.A., van den Bogaard P., Heydolph K., Alvarado G., Protti M., Strauch W. (2008) Arc parallel flow in the mantle wedge beneath Costa Rica and Nicaragua, *Nature* **451**, 1094-1097

Hoernle K., Hauff F., Kokfelt T.F., Haase K., Garbe-Schönberg C.-D. and Werner R. (2011) On- and off-axis chemical heterogeneities along the South Atlantic Mid-Ocean Ridge (5-11°S): Shallow or deep recycling of ocean crust and/or intraplate volcanism? *Earth Planet Sci Lett* **306**, 86-97

Hofmann A.W., Jochum K.P., Seufert M. and White W.M. (1986) Nb and Pb in oceanic basalts: new constraints on mantle evolution, *Earth Planet Sci Lett* **79**, 33-45

Ito E., White W.M., von Drach V., Hofmann A.W. and James D.E. (1980) Isotopic studies of ocean ridge basalts, Carnegie Institute, DTM, annual report director, 465-471

Ito E., White W.M. and Goepel C. (1987) The O, Sr, Nd and Pb isotope geochemistry of mid-oceans ridge basalts, *Chem Geol* **62**, 157-176

Jacques G., Hoernle K., Gill J.B., Hauff F., Wehrmann H., Garbe-Schönber D., van den Bogaard P., Bindeman I. And Lara L.E. (2013) Across-arc geochemical variations in the Southern Volcanic Zone, Chile (34.5-38°S): Constraints on Mantle wedge and source input compositions, *Geochim Cosmochim Ac* **123**, 218-243

Jicha B.R., Singer B.S., Beard B.L., Johnson C.M., Moreno-Roa H. and Naranjo J.A. (2007) Rapid magma ascent and generation of ^{230}Th excesses om the lower crust at Puyehue-Cordón Caulle, Southern Voclanic Zone, Chile, *Earth Planet Sci Lett* **255**, 229-242

Kay S.M., Gorring M. and Ramos V.A. (2004) Magmatic sources, setting and causes of Eocene to recent Patagonian plateau magmatism (36° to 52°S latitude), *Revista de la Asociación Geológica Argentina* **59**, 556-568, 2004

Kay S.M., Ardolino A.A., Gorring M.L. and Ramos V.A. (2007) The Somuncura Large Igneous Province in Patagonia: Interaction of a transient mantle thermal anomaly with a subducting slab, *J Petrol* **48**, 43-77

Kay S.M., Jones H.A. and Kay R.W. (2013) Origin to Tertiary to Recent EM- and subduction-like chemical and isotopic signatures in Auca Mahuida region (37°-38°S) and other Patagonian plateau lavas, *Contrib Mineral Petrol* **166**, 165-192

Kelley K.A., Plank T., Ludden J. and Staudigel H. (2003) Composition of altered oceanic crust at ODP Sites 801 and 1149, *Geochem Geoph Geosy* **4**

Kelley K.A., Plank T., Grove T.L., Stolper E.M., Newman S. and Hauri E. (2006) Mantle melting as a function of water content beneath back-arc basins, *J Geoph Res* **111**

Kimura J.-I., van Keken P.E., Hacker B.R., Kawabata H., Yoshida T. and Stern R.J. (2009) Arc Basalt Simulator version 2, a simulation for slab dehydration and fluid-fluxed mantle melting for arc basalts: Modeling scheme and implication, *Geochem Geoph Geosy* **10**

Kimura J.-I., Kent A.J.R., Rowe M.C., Katakuse M., Nakano F., Hacker B.R., van Keken P.E., Kawabata H. and Stern R.J. (2010) Origin of cross-chain geochemical variation in Quaternary lavas from the northern Izu arc: Using a quantitative mass balance approach to identify mantle sources and mantle wedge processes, *Geochem Geoph Geosy* **11**

Kingsley R.H., Jakobsson S.P., Gable C.W. and Schilling J.G. (2007) Hafnium, Neodymium and Strontium isotope and parent-daughter element systematic in basalts from the plume-

ridge interaction system of the Salas y Gomes seamount chain and Easter microplate, *Geochem Geoph Geosy* **8**

Klein E.M and Karsten J.L (1995) Ocean-ridge basalts with convergent margin geochemical affinities from the Chile Ridge, *Nature* **374**, 52-57

Krolikowska-Ciaglo S., Hauff F. and Hoernle K. (2005) Sr-Nd isotope systematics in 14–28 Ma low-temperature altered mid-ocean ridge basalt from the Australian Antarctic Discordance, Ocean Drilling Program Leg 187, *Geochem Geoph Geosy* **6**

Le Maitre R.W., Bateman P., Dudek A., Keller J., Lameyre Le Bas M.J., Sabine P.A., Schmid R., Sorensen H., Streckeisen A., Woodley A.R. and Zanettin B. (1989) A classification of igneous rocks and glossary of terms, Blackwell, Oxford

López-Escobar L., Cembrano J. and Moreno H. (1995) Geochemistry and tectonics of the Chilean Southern Andes basaltic Quaternary volcanism (37-46°S), *Revista Geológica de Chile* **22**, 219-234

Lucassen F., Trumbull R., Franz G., Creixell C., Vásquez P., Romer R.L. and Figeroa O. (2004) Distinguishing crustal recycling and juvenile additions at active continental margins : the Paleozoic to recent compositional evolution of the Chilean Pacific margin (36-41°S), *J S Am Earth Sci* **17**, 103-119

Lucassen F., Wiedicke M. and Franz G. (2010) Complete recycling of a magmatic arc: evidence from chemical and isotopic composition of Quaternary trench sediments in Chile (36-40°S), *Int J Earth Sci* **99**, 687-701

MacDougall J.D. and Lugmair G.W. (1986) Sr and Nd isotopes in basalts from the East Pacific Rise: significance for mantle heterogeneity, *Earth Planet Sci Lett* **77**, 273-284

Mahoney J.J., Sinto J.M., Kurz M.D., MacDougall J.D., Spencer K.J. and Lugmair G.W. (1994) Isotope and trace element characteristics pf a super-fast spreading ridge: East Pacific Rise 13-23°S, *Earth Planet Sci Lett* **121**, 171-191

Massaferro G.I., Haller M.J., D'Orazio M. and Alric V.I. (2006) Sub-recent volcanism in Northern Patagonia: A tectonomagmatic approach, *J Volcanol Geoth Res* **155**, 227-243

Mattey D., Lowry D. and Macpherson C. (1994) Oxygen isotope composition of mantle peridotite, *Earth Planet Sci Lett* **128**, 231-241

McMillan N.J., Harmon R.S., Moorbath S., Lopez-Escobar L. and Strong D.F. (1989) Crustal sources involved in continental arc magmatism: A case study of volcan Mocho-Choshuenco, southern Chile, *Geology* **17**, 1152-1156

Morris J.D., Leeman W.P. and Tera F. (1990) The subducted component in island arc lavas constraints from Be isotopes and B-Be systematics, *Nature* **344**, 31-36

Naranjo J.A. and Stern C.R. (2004) Holocene tephrochronology of the southernmost part (42°30'-45°S) of the Andean Southern Volcanic Zone, *Revista Geológica de Chile* **31**, 225-240

Newsom H.E., White W.M., Jochum K.P. and Hofmann A.W. (1986) Siderophile and chalcophile element abundances in oceanic basalts, Pb isotopes evolution and growth of the Earth's core, *Earth Planet Sci Lett* **80**, 299-313

Norabuena E., Leffer-Griffin L., Mao A., Dixon T., Stein S., Sacks S., Ocola L. And Ellis M. (1998) Space geodetic observations of Nazca-South America convergence across the central Andes, *Science* **279**, 358-362

Pearce J.A. (2008) Geochemical fingerprinting of oceanic basalts with applications to Ophiolite classification and the search for Archean oceanic crust, *Lithos* **100**, 14-48

Pécskay Z., Haller M.J. and Németh K. (2007) Preliminary K/Ar Geochronology of the Crater basalt Volcanic Field (CBVF), northern Patagonia, *Revista de la Asociación Geológica Argentina* **62**, 25-29

Plank T. (2011) The chemical composition of subducting sediments, Chapter for Treatise on Geochemistry

Ranero C.R., Phipps Morgan J., McIntosh K. and Reichert C. (2003) Bending-related faulting and mantle serpentinization at the Middle America trench, *Nature* **425**, 367-373

Ranero C.R., Villasenor A., Phipps Morgan J. and Weinrebe W. (2005) Relationship between bend-faulting at trenches and intermediate-depth seismicity, *Geochem Geoph Geosy* **6**

Ranero C.R., Huene R.v., Weinrebe W. and Reichert C. (2006) Tectonic Processing along the Chile Convergent Margin, In: O. Oncken, G. Chong, G. Franz, P. Giese, H.-J. Götze, V. Ramos M. Strecker, and P. Wigger (Eds): The Andes Active Subduction Orogeny, Frontiers in Earth Science. Springer Verlag, Berlin, 91-121

Reubi O., Bourdon B., Dungan M.A., Koornneef J.M., Sellés D., Langmuir C.H. and Aciego S., (2011) Assimilation of the plutonic roots of the Andean arc controls variations in U-series disequilibria at Volcan Llaima, Chile, *Earth Planet Sci Lett* **303**, 37-47

Roy-Barman M., Wasserburg G.J., Papanastassiou D.A. and Chaussidon M. (1998) Osmium isotopic compositions and Re-Os concentrations in sulfide globules from basaltic glasses, *Earth Planet Sci Lett* **154**, 331-347

Rüpke L.H., Phipps Morgan J., Hort M. and Connolly J.A.D. (2002) Are the regional variations in Central American arc lavas due to differing basaltic versus peridotitic slab sources of fluids?, *Geology* **30**, 1035-1038

Rüpke L.H., Phipps Morgan J., Hort M. and Connolly J.A.D. (2004) Serpentine and the subduction zone water cycle, *Earth Planet Sci Lett* **223**, 17-37

Sellés D., Ródriguez A.C., Dungan M.A, Naranjo J.A. and Gardeweg M. (2004) Geochemistry of Neva de Longaví volcano (36.2°S): a compositionally atypical arc volcano in the Southern Volcanic Zone of the Andes, *Revista Geológica de Chile* **31**, 293-315

Sigmarsson O., Condomines M., Morris J.D. and Harmon R.S. (1990) Uranium and 10be enrichments by fluids in Andean arc magmas, *Nature* **346**, 163-165

Sigmarsson O., Chmeleff J., Morris J. and López-Escobar L. (2002) Origin of 226Ra-230^{Th} disequilibria in arc lavas from southern Chile and implications for magma transfer time, *Earth Planet Sci Lett* **196**, 189-196

Stern C.R., Frey F.A., Kiyoto F., Zartman R.E., Peng Z., Kurtis Kyser T. (1990) Trace-element and Sr, Nd, Pb, and O isotopic composition of Pliocene and Quaternary alkali basalts of the Patagonian Plateau lavas of southernmost South America. *Contrib Mineral Petrol* **104**, 294-308

Stern C.R. (2004) Active Andean volcanism: its geologic and tectonic setting, *Revista Geológica de Chile* **31**, 161-206

Sturm M., Klein E.M., Graham D. And Karsten J.L. (1999) Age constraints on crustal recycling to the mantle beneath the Southern Chile Ridge: He-Pb-Sr-Nd isotopes systematic, *J Geoph Res* **104**, 5097-5114

Sun S.-s. and McDonough W.F. (1989) Chemical and isotopic systematic of oceanic basalts: implications for mantle composition and processes, in Magmatism in ocean basins (Saunders A.D. and Norry M.J., editors) Geological Society, London special publication **42**, 313-345

Tagiri M., Moreno H., López-Escobar L. and Notsu K. (1993) Two magma types of the high-alumina basalt series of Osorno Volcano, Southern Andes (41°06'S) – plagioclase dilution effect, *J Mineral Petrol Eco Geol* **88**, 359-371

Tassara A., Götze H.J., Schmidt S. and Hackney R. (2006) Three-dimensional density model of the Nazca plate and the Andean continent margin, *J Geoph Res* **111**

Tebbens S.F. and Cande S.C. (1997) Southeast Pacific tectonic evolution from early Oligocene to present, *J Geoph Res* **102**, 12,061-12,084

Tebbens S.F., Cande S.C., Kovacs L., Parra Labrecque J.L. and Vergara H. (1997) The Chile ridge: a tectonic framework, *J Geoph Res* **102**, 12,035-12,059

Tormey D.R., Hickey-Vargas R., Frey F.A. and López-Escobar L. (1991) Recent lavas from the Andean volcanic front (33 to 42°S); Interpretations of along-arc compositional variations, *Geol Soc Am* special paper **265**, 57-77

Turner S., Handler M., Bindeman I.N. and Katsuhiko S. (2009) New insights into the origin of O-Hf-Os signatures in arc lavas from Tonga-Kermadec, *Chem Geol* **266**, 187-193

Valley J. W., Kitchen N., Kohn M. J., C.R. N. and Spicuzza M. J. (1995) UWG-2, a garnet standard for oxygen isotope ratios: strategies for high precision and accuracy with laser heating, *Geochim Cosmochim Ac* **59**, 5223-5231

Vallier T.L., Jenner G.A., Frey F.A., Gill, J.B., Davis A.S., Volpe A.M., Hawkins J.W., Morris J.D., Cawood P.A., Morton J.L., Scholl D.W., Rautenschlein M., White W.M., Williams R.W., Stevenson A.J. and White L.D. (1991) Subalkaline andesite from Valu Fa Ridge, a back-arc spreading center in southern Lau Basin: petrogenesis, comparative chemistry, and tectonic implications, *Chem Geol* **91**, 227-256

Van Keken P.E., Hacker B.R., Syracuse E.M. and Abers G.A. (2011) Subduction factory: 4. Depth-dependent flux of H_2O from subducting slabs worldwide, *J Geoph Res* **116**

Varekamp J.C., Hesse A. and Mandeville C.W. (2010) Back-arc basalts from the Loncopue graben (Province of Neuquén, Argentina), *J Volcanol Geoth Res* **197**, 313-328

Völker D., Reichel T., Wiedicke M. and Heubeck C. (2008) Turbidites deposited on Southern Central Chilean seamounts: Evidence for energetic turbidity currents, *Mar Geol* **251**, 15-31

Völker D., Kutterolf S. and Wehrmann H. (2011) Comparative mass balance of volcanic edifices at the Southern Volcanic Zone of the Andes between 33°S and 46°S, J *Volcanol Geoth Res* **205**, 114-129

Wade J.A, Plank T., Stern R.J, Tollstrup D.L., Gill J.B., O'Leary J.C., Eiler J.M., Moore R.B., Woodhead J.D., Trusdell F., Fisher T.P. and Hilton D.R. (2005) The May 2003 eruption of Anatahan volcano, Mariana Islands: Geochemical evolution of a silicic island-arc volcano, *J Volcanol Geoth Res* **146**, 139-170

Watt S.F.L., Pyle D.M., Tamsin A.M. and Naranjo J.A. (accepted, 2013) Arc magma compositions controlled by linked thermal and chemical gradients above the subducting slab, *Geoph Res Lett* DOI: 10.1002/grl.50513

Wehrmann H., Hoernle K., Garbe-Schönberg C.-D., Jacques G., Mahlke J. and Schumann K. (accepted, 2014) Fluids in volcanic arc systems: Insights from trace element geochemistry of mafic to intermediate volcanic rocks, *Int J Earth Sci*

Wehrmann H., Hoernle K., Jacques G., Garbe-Schönberg D., Schumann K., Mahlke J. and Lara L. (in rev) Sulphur and chlorine geochemistry of mafic to intermediate tephras from the

Chilean Southern Volcanic Zone (33-43°S) compared with those from the Central American Volcanic Arc, *Int J Earth Sci*

White W.M., Hofmann A.W. and Puchelt H. (1987) Isotope geochemistry of Pacific Mid-Ocean Ridge basalts, *J Geoph Res* **92**, 4881-4893

Workman R.K. and Hart S.R. (2005) Major and trace element composition of the depleted MORB mantle (DMM), *Earth Planet Sci Lett* **231**, 53-42

Table captions:

Table 1. New Sr-Nd-Hf-Pb isotope data for the samples described in the supplementary Table 1. See the text for results for reference materials.

Table 2. O isotope data from olivine, plagioclase, groundmass (glass or matrix) and $\delta^{18}O_{melt}$. $\delta^{18}O_{melt}$ was calculated by adding 0.6‰ to the olivine or subtracting 0.1 to the plagioclase value.

Table 3. Sediment (SED), altered oceanic crust (AOC) and depleted MORB Mantle (DMM) compositions used for the Arc Basalt Simulator 3 calculations. (*) See Table 4 for values used in calculation of the slab melt composition.

Table 4. Mixing parameters and results for one stratovolcano sample (CL 170) from the Arc Basalt Simulator 3. AOC = Altered Oceanic Crust, SED = Sediment.

Figure captions:

Figure 1. (A) Map of the Southern Volcanic Zone (SVZ) with volcanic front volcanoes denoted with yellow triangles. The black thick line represents the boundary between Chile and Argentina. (B) Map of the Central SVZ and the northern part of the Southern SVZ, from 38°S to 43°S. Green squares = CSVZ stratovolcanoes. Green squares with white cross = monogenetic cinder cones. Blue diamonds stand for the Transitional SVZ. Open squares = Backarc lavas. Yellow triangles = other Quaternary volcanoes. In (A) and (B): Grey filled circles = major cities. The red arrows show the relative movement of the Nazca plate beneath the South American plate. FZ = fracture zone. The ETOPO1 map source is from NOAA, modified (Amante and Eakins, 2009).

Figure 2. (a) Total Alkali versus Silica [TAS] after Le Maitre et al. (1989). CSVZ samples range in composition from basalt to trachyandesite. The cinder cones are primarily basaltic. (b) SiO_2 versus K_2O after Gill (1981). The VA samples are medium-K and tholeiitic. Most BA samples are alkali basalts to trachybasalts. CSVZ data are from Wehrmann et al. (2014) and (in rev) and this study. TSVZ data are from Jacques et al. (2013).

Figure 3. MgO versus major element oxides. The CSVZ VA trends overlap the TSVZ VA and have lower Na_2O and K_2O at a given MgO content. The cinder cones are least differentiated of the VA. BA samples extend to higher MgO, CaO and to lower SiO_2, Al_2O_3 compared to the VA. BA samples generally have lower SiO_2 and higher incompatible minor oxide abundances (Na_2O,

TiO_2, K2O and P_2O_5) at a given MgO content than VA samples. Data source are the same as in Figure 2.

Figure 4. Multi-element diagram normalized to normal mid-ocean-ridge basalt (N-MORB) of Sun and McDonough (1989), showing the differences between: (a) the average CSVZ stratovolcanoes and cinder cones, (b) the average CSVZ stratovolcanoes, CSVZ BA, CSVZ MEBA (more-enriched BA samples), and TSVZ BA, and (c) the average CSVZ stratovolcanoes, TSVZ VA, the average Chilean trench sediment at 40°S from Plank (2011) and the AOC component from Kelley et al. (2003). All VA samples show typical subduction zone trace element signatures with e.g. K and Pb peaks and Nb and Ta troughs. Cinder cones overall have a less pronounced subduction signature than the stratovolcanoes. The Apagado cinder cone sample has the least enriched pattern in all elements, except Nb, K, Sr and Ti. The BA shows a similar pattern but with the least subduction signature, especially in the more-enriched backarc (MEBA) group, defined based on more-enriched isotopic composition. The CSVZ stratovolcanoes have lower contents of all incompatible elements between Cs and Pb but higher HREE and Y abundances than the TSVZ VA. All samples follow the trench sediment pattern closely. Data sources are the same as in Figure 2.

Figure 5. (a) La/Yb versus U/Th. The CSVZ and TSVZ VA samples form a negative correlation. The CSVZ stratovolcanoes have the highest U/Th ratios, reflecting the highest slab fluid signal, and the lowest La/Yb, reflecting the highest degrees of melting (see also Dzierma et al., 2012). The cinder cones are more similar in composition to the TSVZ VA. The BA samples show a similar range in U/Th but are shifted to higher La/Yb, reflecting lower percent melting relative to

VA samples. (b) Nb/Yb versus Ce/Pb. The SVZ VA and BA samples form a positive correlation with the BA extending to higher Ce/Pb and Nb/Yb, consistent with a higher slab component and higher degrees of melting in the SVZ VA in general, and in the CSVZ in particular. Data sources are the same as in Figure 2. Arrow points to additional BA data from Stern et al. (1990).

Figure 6. Nb/Yb versus Th/Yb after Pearce (2008). MORB and OIB define the positive trend labeled MORB-OIB array, reflecting greater mantle source enrichment at higher ratios along the array. All SVZ VA and many BA samples plot above the line indicating Th enrichment primarily through addition of a slab component to the source, since evidence for crustal assimilation is minimal in these samples. The CSVZ BA samples lie slightly above the MORB-OIB array, indicating small amounts of a slab component in their source. The isotopically more-enriched (ME) BA samples lie within the MORB-OIB array, consistent with the absence of a slab component in them, as is also the case for some of the TSVZ BA samples. The decreasing Nb/Yb ratios from the BA samples to the TSVZ VA to the CSVZ VA cinder cones to CSVZ VA stratovolcanoes could reflect derivation through increasing degrees of melting and/or from increasingly more depleted sources. The white dots show the results of the ABS melting model presented in Section 5.7 as a function solely of temperature, starting at 1200°C and increasing to 1300°C in 10°C increments. The temperature range corresponds to an increase in the percent melting from 3 to 9%. Data sources are the same as in Figure 2. The Chilean trench sediment field is from Jacques et al. (2013) and Lucassen et al. (2010). CSVZ literature data are from Gerlach et al. (1988) and Hickey-Vargas et al. (1989); BA data are from Stern et al. (1990).

Figure 7. Nb/U versus Ce/Pb. The CSVZ stratovolcano samples overlap the TSVZ VA, while the monogenetic cinder cone samples have more mantle-like Ce/Pb and Nb/U ratios, with the typical mantle range (dashed box) represented by the typical MORB and OIB range after Hofmann et al. (1986). The CSVZ BA samples extend to even more mantle-like values. Data source are the same as in Figure 6.

Figure 8. $^{87}Sr/^{86}Sr$ versus $^{143}Nd/^{144}Nd$. The CSVZ VA and TSVZ VA samples form a rough negative array but most of the CSVZ stratovolcano data form a cluster with elevated $^{87}Sr/^{86}Sr$ and/or $^{143}Nd/^{144}Nd$ compared to the CSVZ cinder cones and the TSVZ VA, which overlap. CSVZ BA and TSVZ BA samples overlap the TSVZ VA, but the MEBA samples are shifted to more enriched compositions. All samples, except some of the MEBA group, plot within the South Atlantic MORB field. The star denotes the "typical" sediment used in modeling (see Figure 13), while the circle shows the average Chilean trench sediment at 40°S of Plank (2011). CSVZ VA literature data are from Harmon et al. 1984), Hickey et al. (1986), Hickey-Vargas et al. (1989), Gerlach et al. (1988). Backarc literature data are from Stern et al. (1990). Trench sediment data are from Lucassen et al. (2010) and Jacques et al. (2013). TSVZ VA data are from Jacques et al. (2013). East Pacific Rise (20-34°S) MORB data are from Fontignie and Schilling (1991), Haase (2002), Hamelin et al. (1984), Hanan and Schilling (1989), Ito et al. (1980), Ito et al. (1987), Kingsley et al. (2007), MacDougall and Lugmair (1986), Mahoney et al. (1994), Newsom et al. (1986) and White et al. (1987). South Atlantic (30-50°S) MORB data are from Andres et al. (2002), Douglas et al. (1999), Fontignie and Schilling (1996), Hanan et al. (1986) and Roy-Barman et al. (1998).

Figure 9. $^{206}Pb/^{204}Pb$ versus (a) $^{207}Pb/^{204}Pb$ and (b) $^{208}Pb/^{204}Pb$. The CSVZ VA samples form a tight positive array similar to the TSVZ VA samples. All samples plot at the base of the trench sediment field. The CSVZ monogenetic cinder cone samples extend to less radiogenic Pb isotopic compositions with the Apagado sample having the least radiogenic Pb of all SVZ VA samples. Excluding the five MEBA samples, the CSVZ BA samples overlap the radiogenic end of the TSVZ BA array and the unradiogenic end of the VA array. The star shows the "typical" sediment used in modeling (see Figure 13), while the circle shows the average Chilean trench sediment at 40°S of Plank (2011). Data sources for TSVZ, sediment and MORBs are the same as for Figure 8. Basement data are from Lucassen et al. (2004). The trench sediment field includes river mouth sediments from Hildreth and Moorbath (1988).

Figure 10. εNd versus εHf. The CSVZ VA samples plot on the same positive array defined by the TSVZ VA samples but the CSVZ VA samples extend to more radiogenic compositions. In both segments, the VA and BA samples form two subparallel trends, the BA having lower εHf at a given εNd. The MEBA samples have the lowest εHf and εNd of all the BA samples. Data sources for MORB are the same as in Figure 8. TSVZ data and sediments are from Jacques et al. (2013).

Figure 11. $\delta^{18}O_{melt}$ versus (a) U/Th and (b) $^{143}Nd/^{144}Nd$. CSVZ stratovolcano samples have lower $\delta^{18}O_{melt}$ values than CSVZ cinder cone and TSVZ VA samples, extending to values below the MORB range. $\delta^{18}O_{melt}$ of our samples form crude negative correlations with Nd isotopes and U/Th ratios. The high U/Th and Nd isotope ratios and low $\delta^{18}O_{melt}$ suggests that the higher fluid flux beneath the CSVZ stratovolcanoes is associated with a more depleted, hydrothermally-

altered source, such as lower oceanic crust or serpentinites. $\delta^{18}O_{melt}$ corresponds to $\delta^{18}O_{ol}$ converted to $\delta^{18}O_{melt}$ by adding 0.6‰. MORB range after Bindeman (2008) and references therein. $\delta^{18}O$ range in island arcs is from Ewart et al., 1987, Turner et al., 2009, Vallier et al., 1991, Wade et al., 2005. Subducted sediments can increase the $\delta^{18}O$ of the mantle source to values above the MORB range. Data sources are the same as in Figure 6.

Figure 12. MgO versus (a) $^{87}Sr/^{86}Sr$, (b) $^{143}Nd/^{144}Nd$ for Llaima, Villarrica and Osorno. The data for the individual volcanoes and for the CSVZ on the whole can be explained by crystal fraction (indicated by horizontal black arrows) without the need to invoke concomitant assimilation (AFC). MgO from our samples from Wehrmann et al. (2014) and (in rev). Data source for Villarrica:, Hickey-Vargas et al., 1989, 2002, Llaima: Hickey et al., 1986, Hickey-Vargas et al., 1989, Reubi et al., 2011, Osorno: Hickey et al., 1986, Tagiri et al., 1993.

Figure 13. $^{87}Sr/^{86}Sr$ versus (a) $^{143}Nd/^{144}Nd$ and (b) $^{206}Pb/^{204}Pb$. The mixing lines show results from a forward mass balance model using the Arc Basalt Simulator 3.10 as explained in the text and using the values summarized in Table 3. The dashed line represents mixing between altered oceanic crust (AOC) and sediment (SED). The thin lines represent mixing between a 22% melt of a 30:70 SED:AOC source on the one hand, and depleted (SAM-D) or enriched (SAM-E) mantle (the two stars) on the other. Mixing with mantle with an intermediate composition between SAM-D and SAM-E (the unlabeled black star) is also shown. The labeled tick marks show the amount of slab component added to the mantle. Slab and mantle melting conditions are described in the text. Partition coefficients and melting modes for the slab and mantle are from Kimura et al. (2010) and given in Table 4.

Figure 1

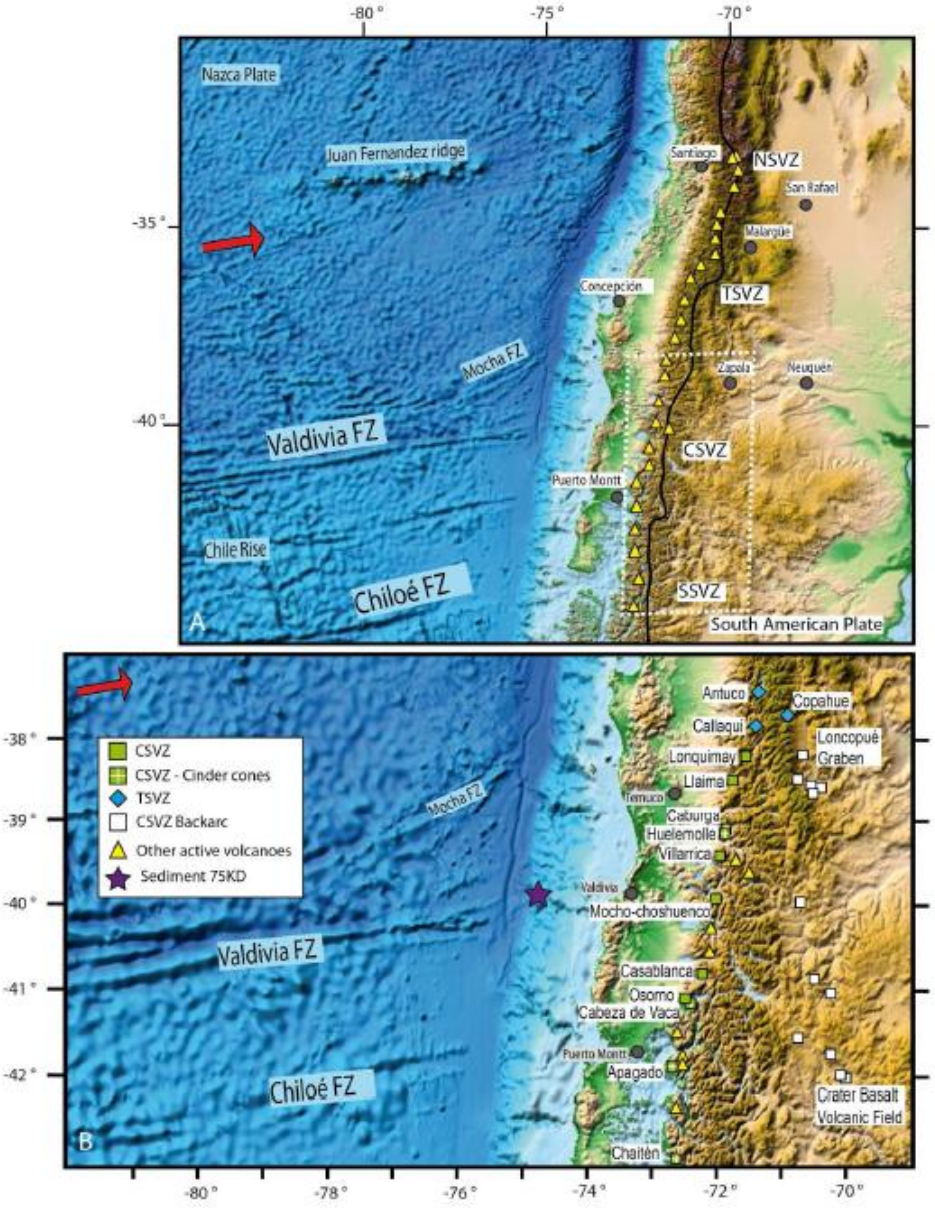

Figure 2

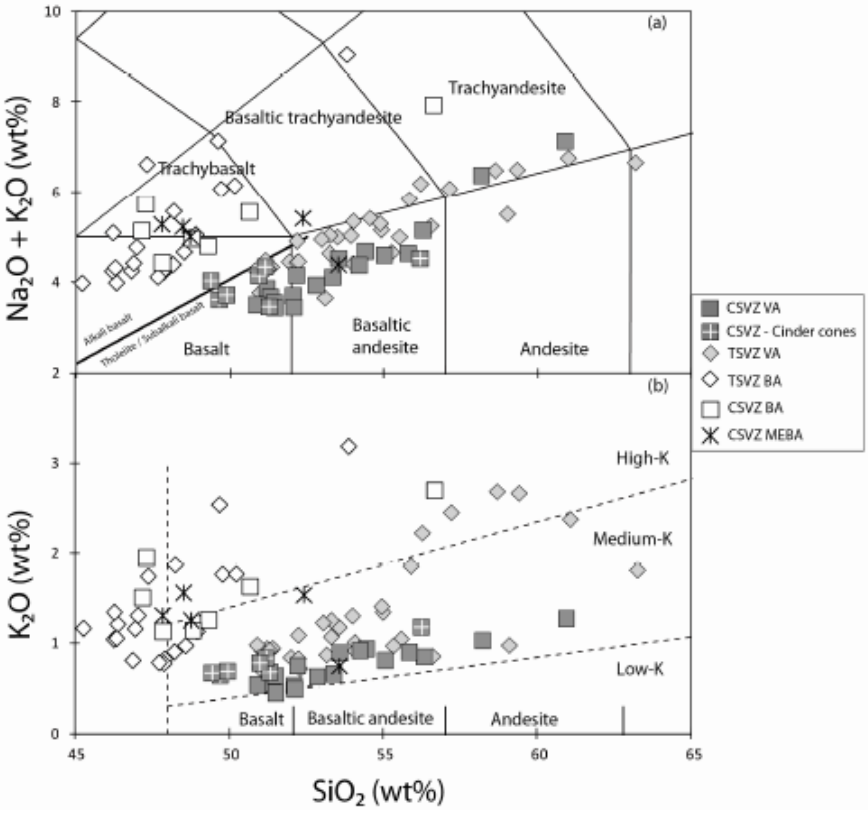

Figure3

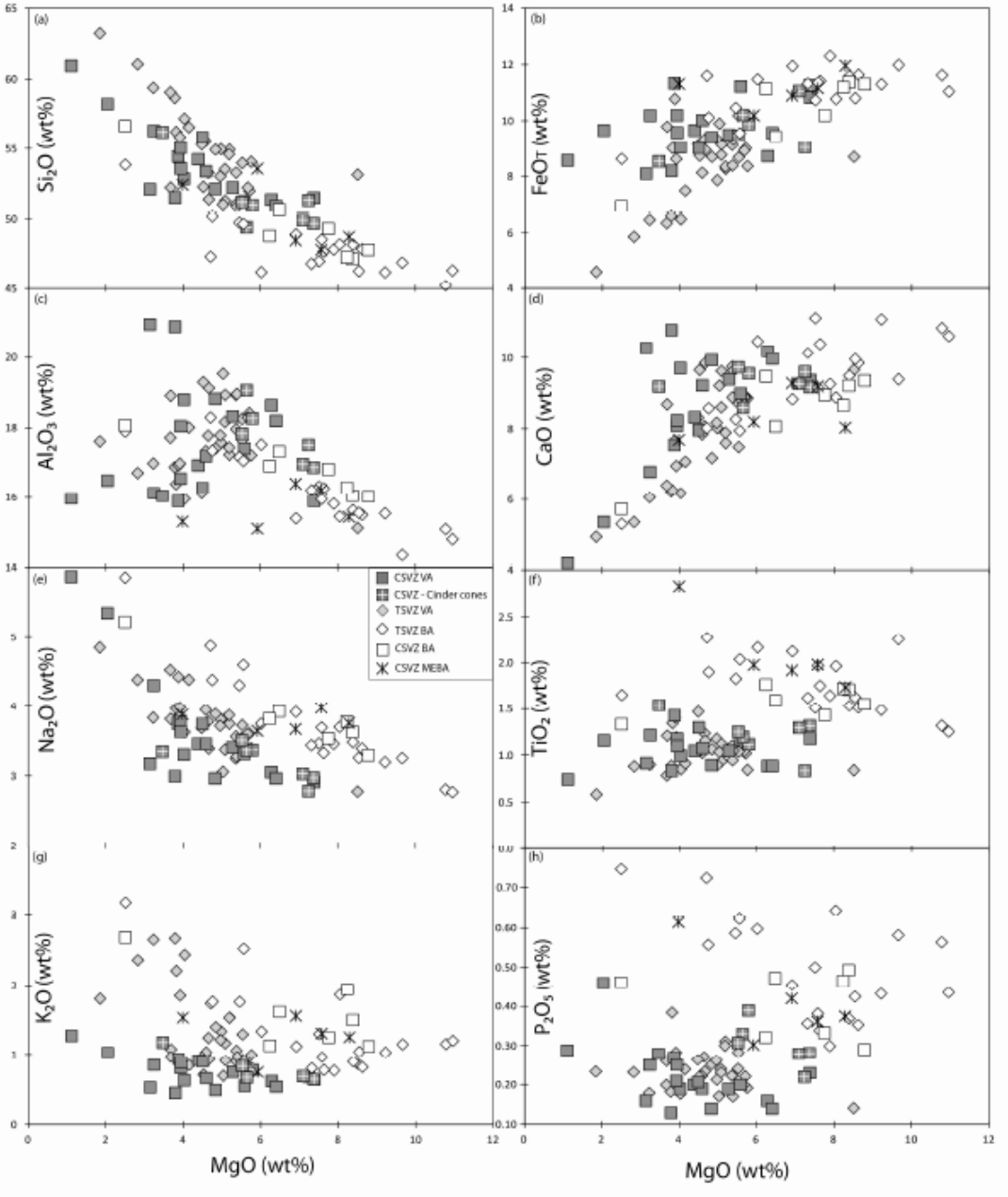

Figure 4

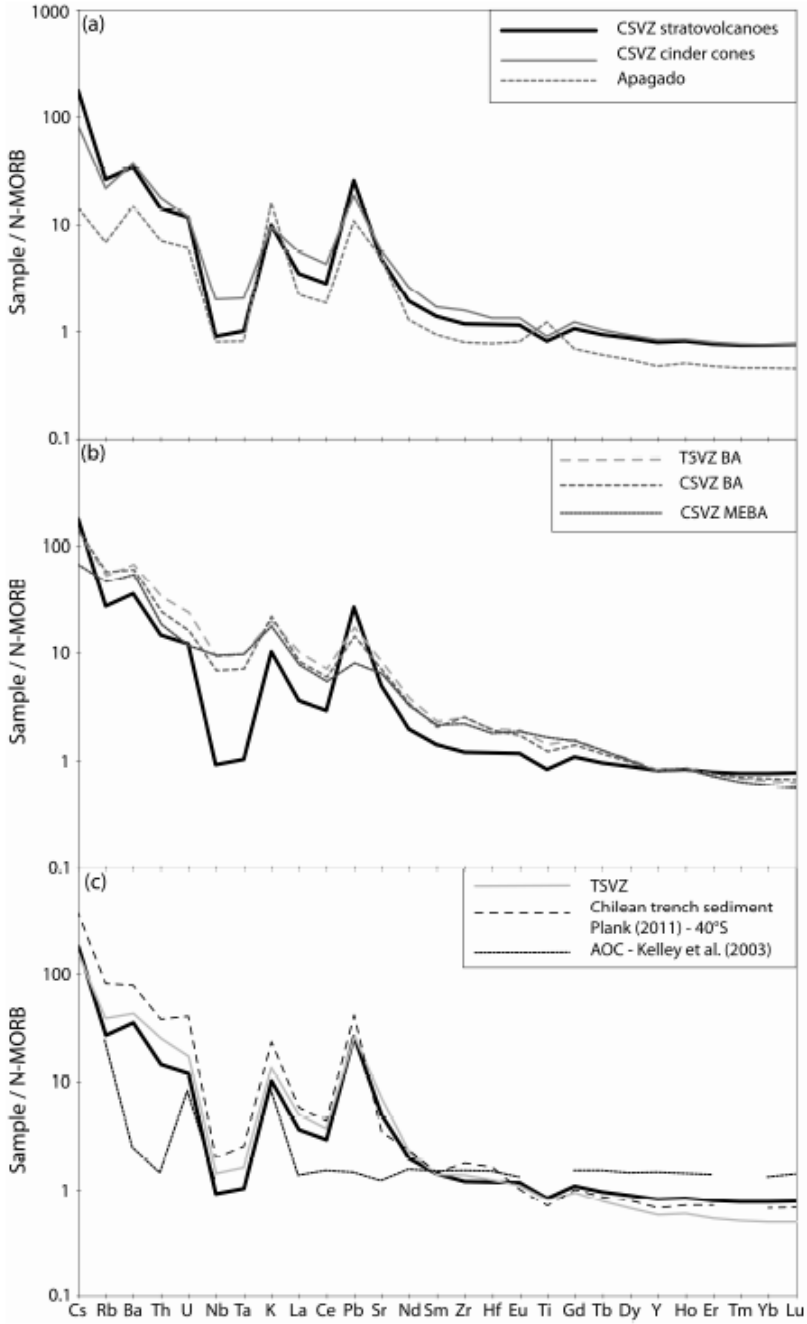

Figure 5

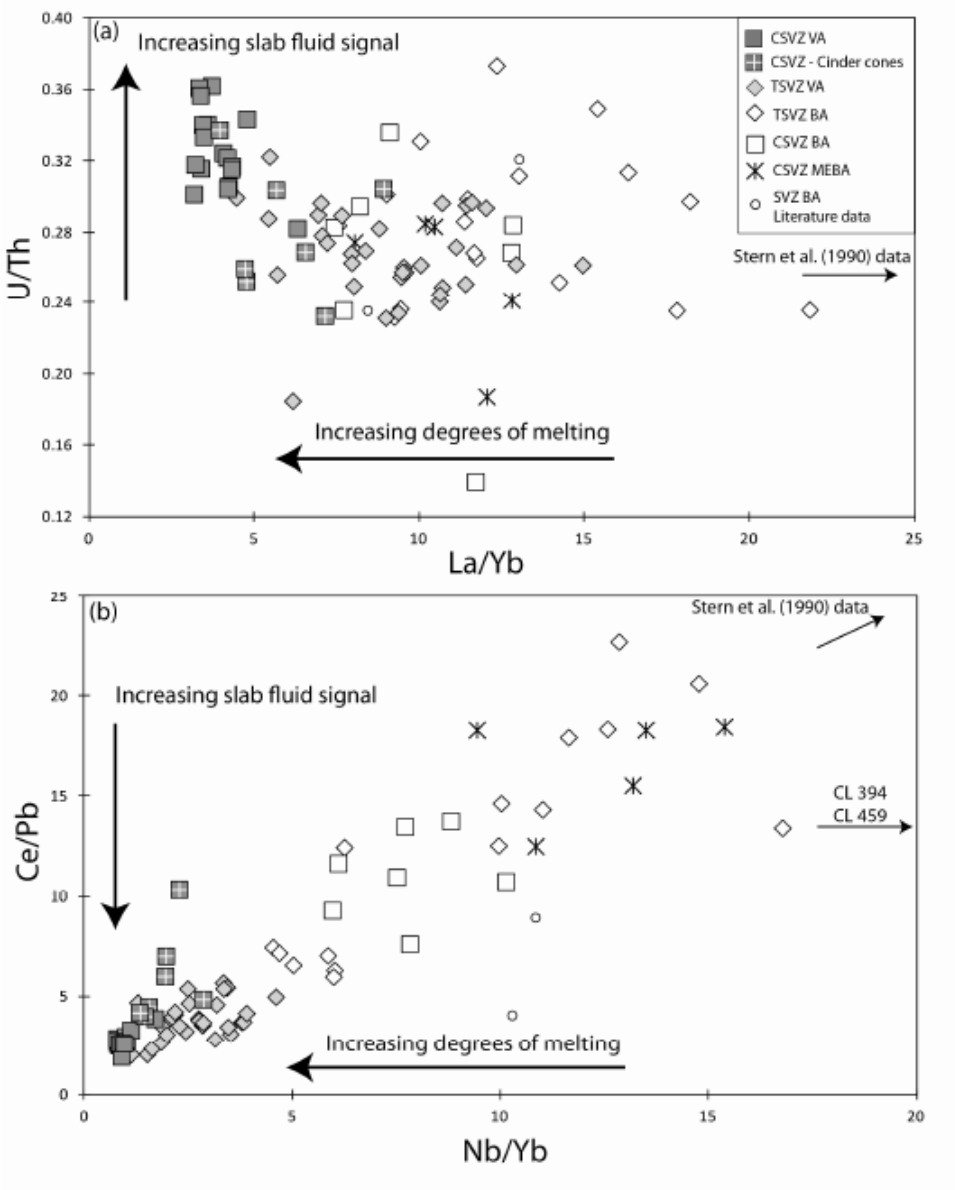

Figure 6

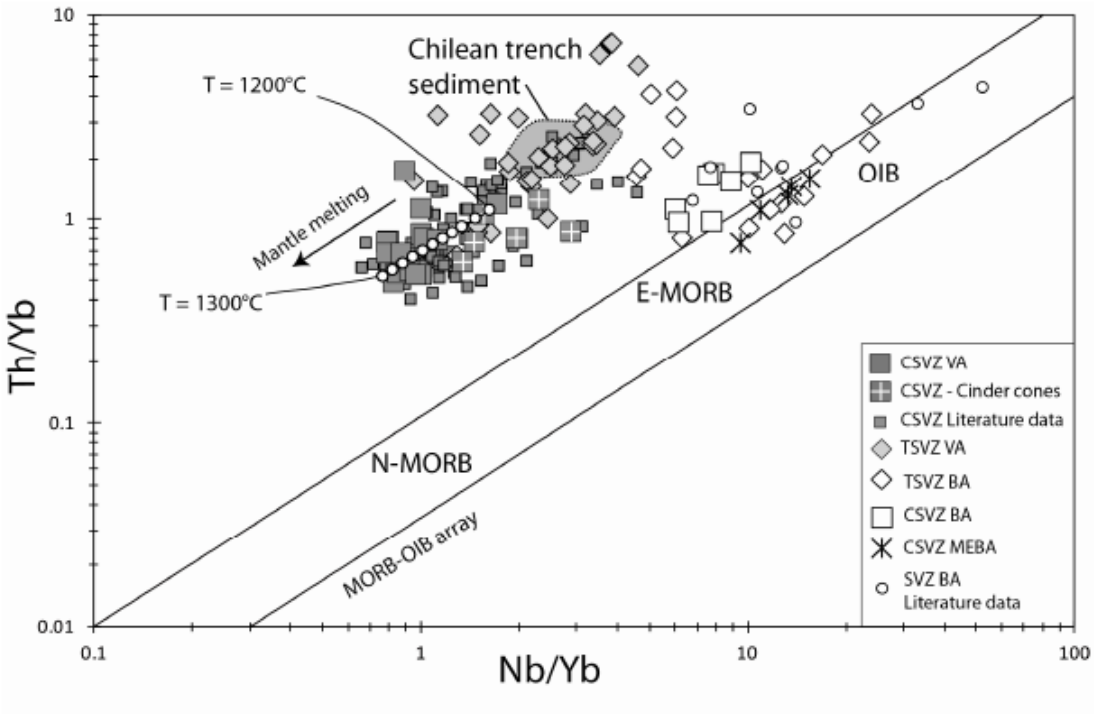

Figure 7

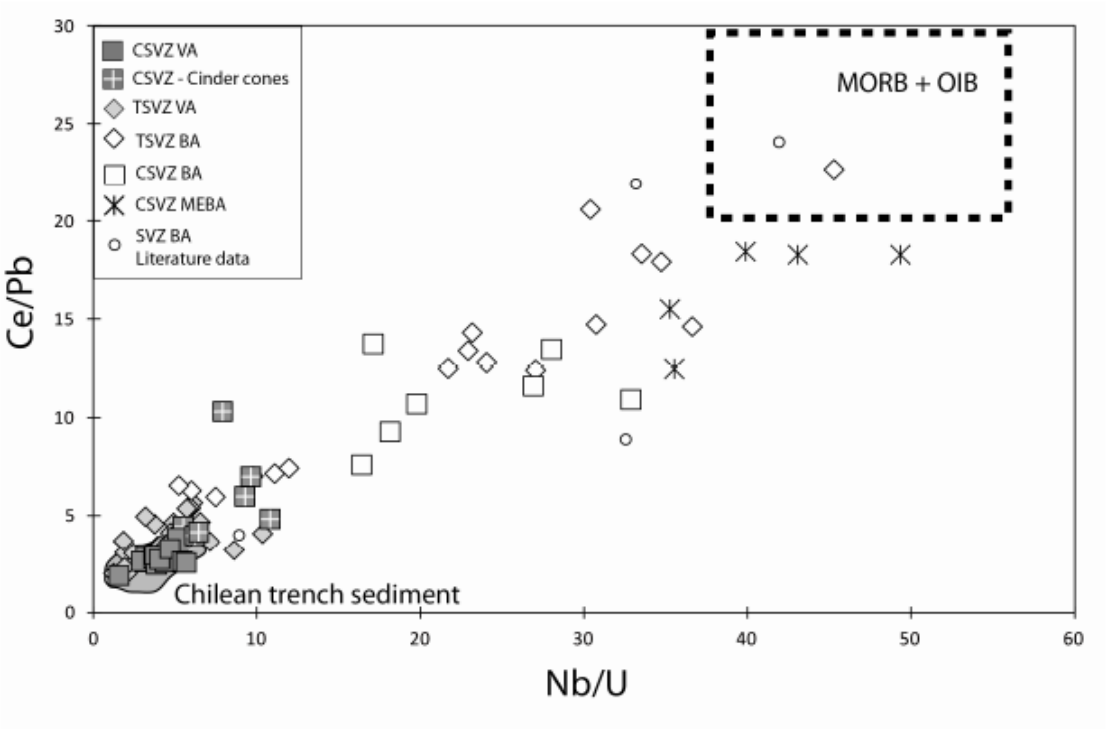

Figure 8

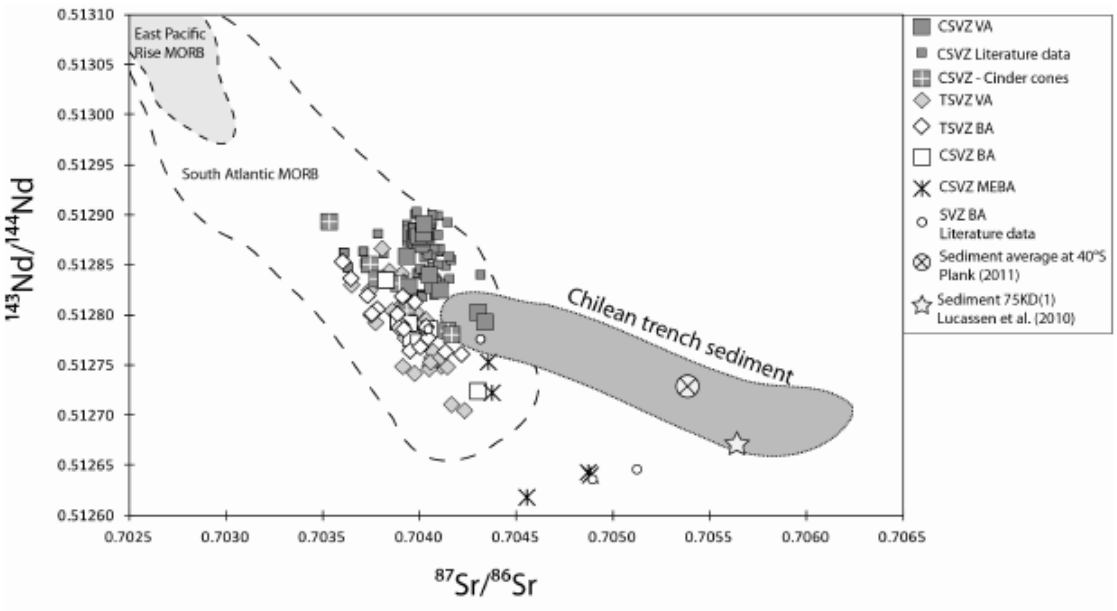

Figure 9

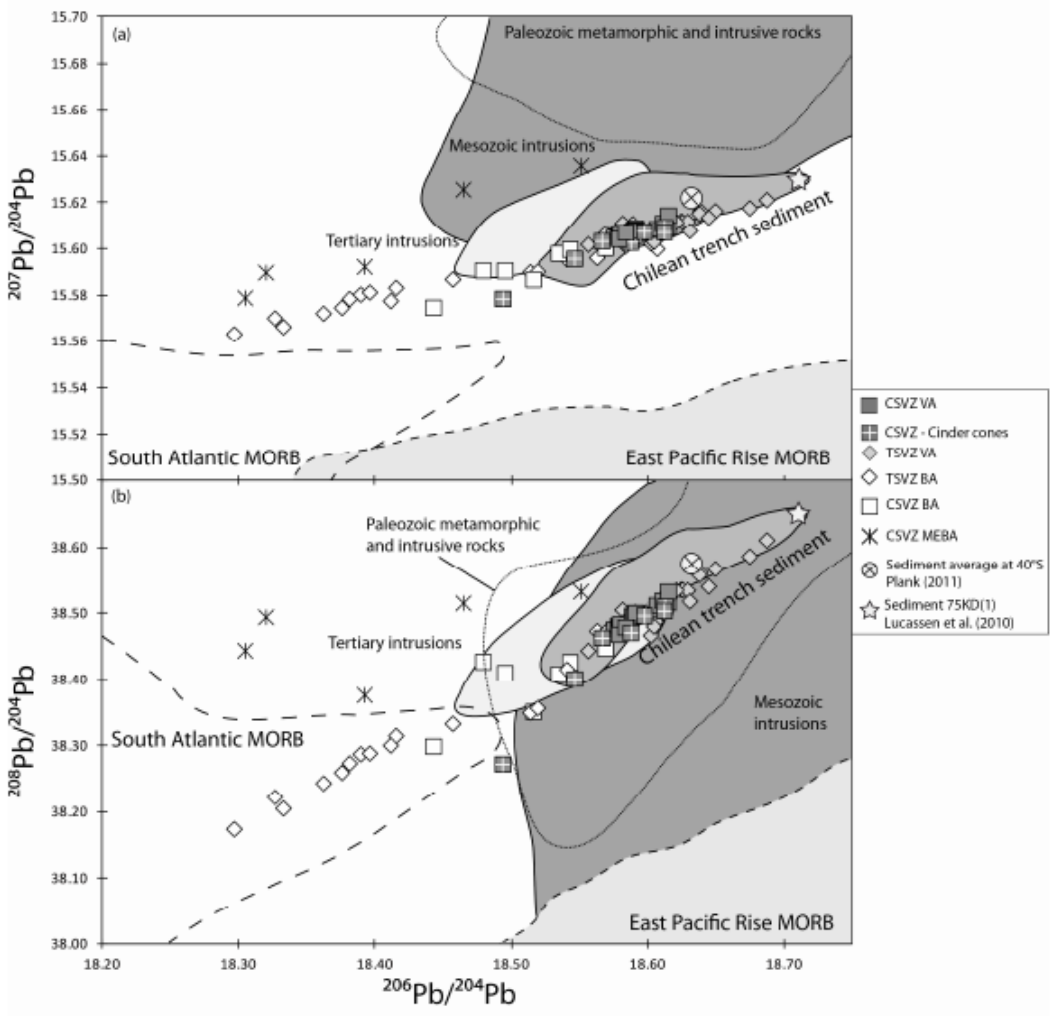

Figure 10

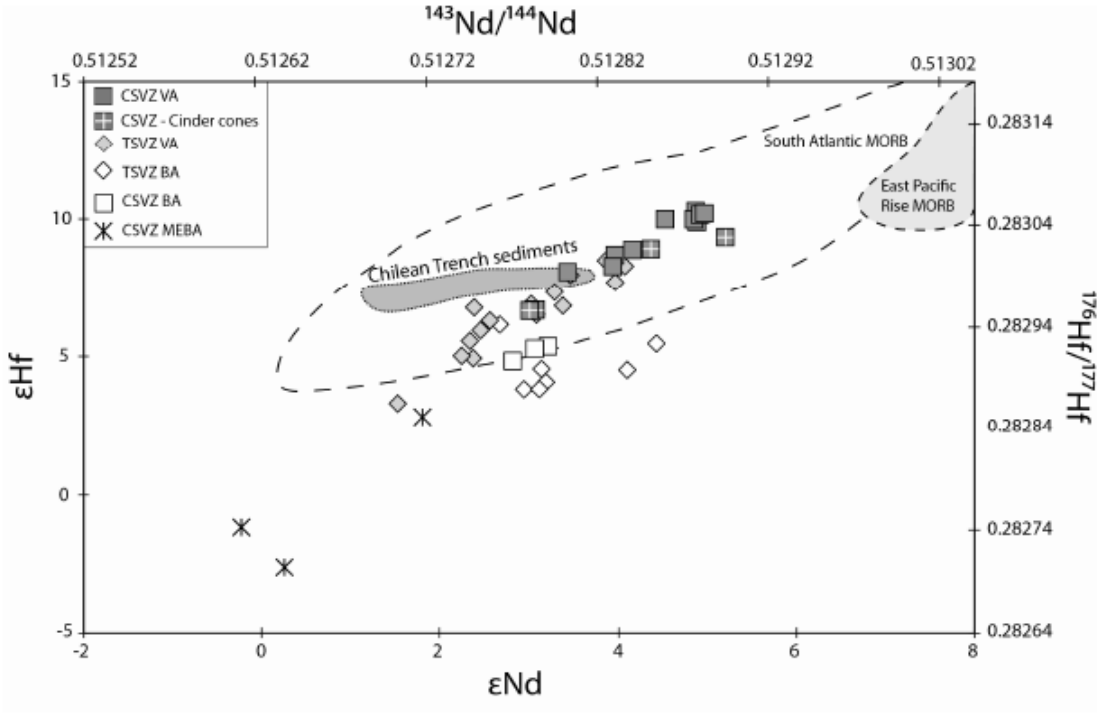

Figure 11

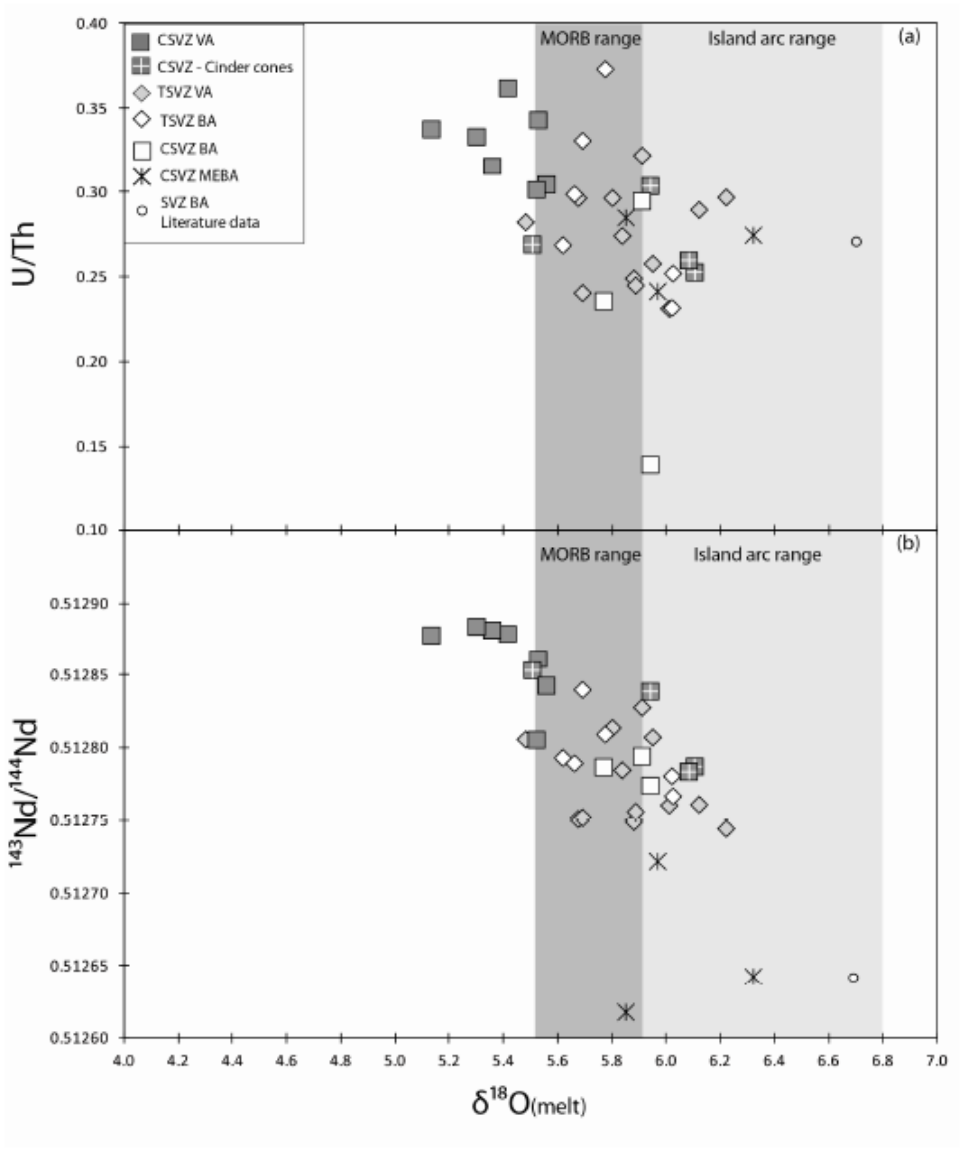

Figure 12

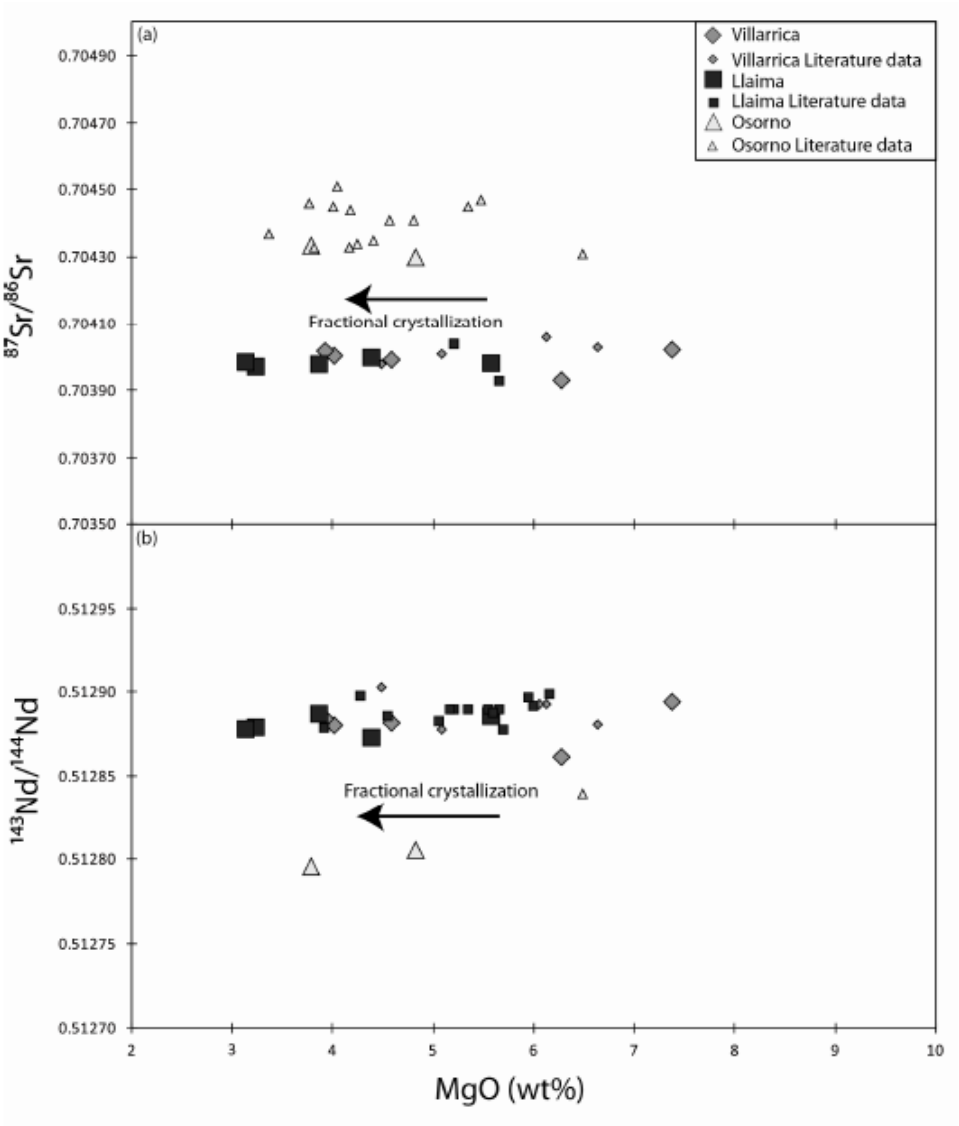

Figure 13

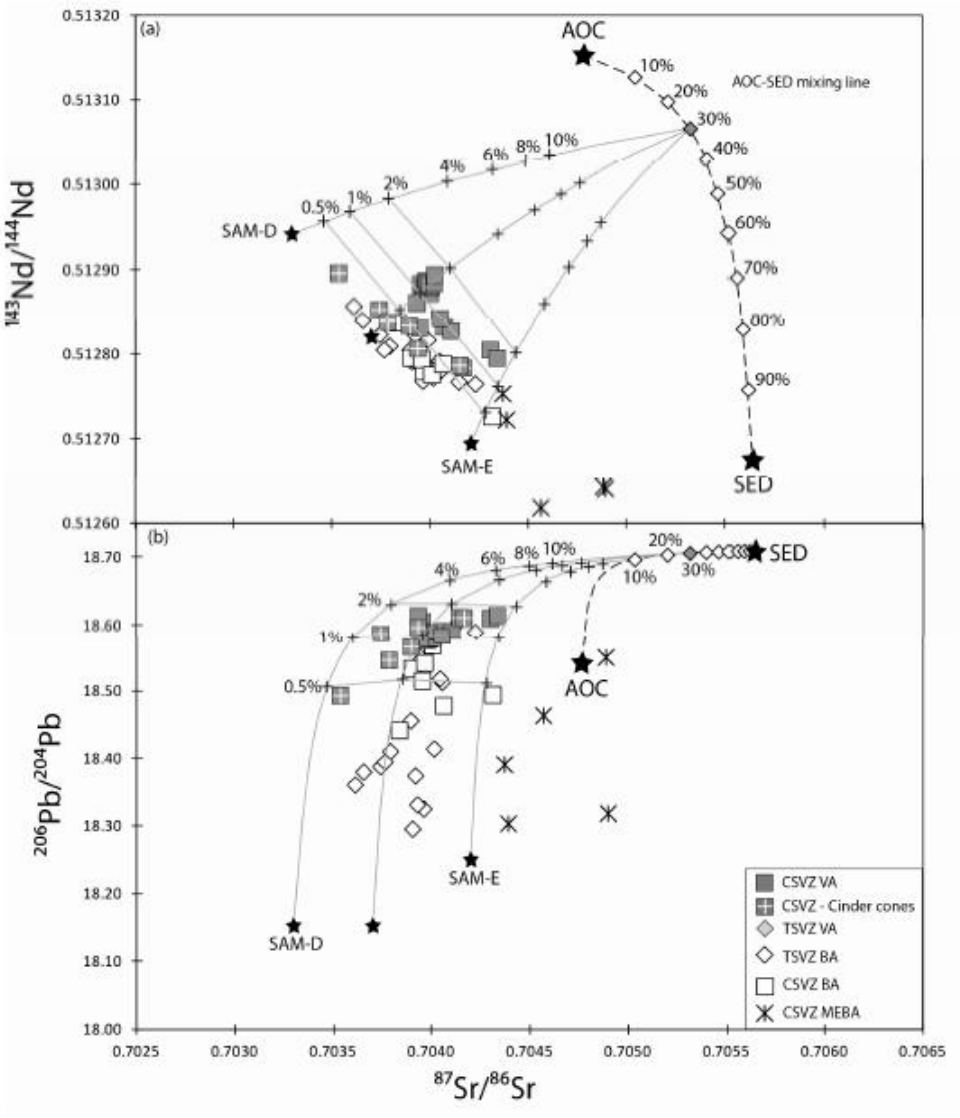

Table 1

Sample number	Sample Location	$^{87}Sr/^{86}Sr$	2σ	$^{143}Nd/^{144}Nd$	2σ	εNd	$^{176}Hf/^{177}Hf$	2σ	εHf	$^{206}Pb/^{204}Pb$	2σ	$^{207}Pb/^{204}Pb$	2σ	$^{208}Pb/^{204}Pb$	2σ
Volcanic Arc															
CL 045	Lonquimay	0.703952	3	0.512880	2	4.88	0.283065	4	9.91	18.6061	7	15.6083	9	38.5061	28
CL 049	Lonquimay	0.703952	3	0.512884	2	4.96				18.6062	30	15.6087	27	38.5121	69
CL 029	Llaima	0.703972	3	0.512879	2	4.86	0.283076	10	10.31	18.5750	12	15.6051	15	38.4765	48
CL 032	Llaima	0.703986	3	0.512878	3	4.84	0.283068	8	10.01	18.5779	10	15.6057	11	38.4811	34
CL 034	Llaima	0.703980	4	0.512887	2	5.02				18.5786	13	15.6053	15	38.4807	48
CL 035	Llaima	0.703982	3	0.512886	2	4.99				18.5789	7	15.6051	9	38.4801	28
CL 036	Llaima	0.703999	3	0.512873	3	4.74				18.5795	7	15.6058	9	38.4839	28
CL 001	Villarrica	0.704005	3	0.512881	3	4.89				18.5908	8	15.6091	9	38.5010	30
CL 006	Villarrica	0.703993	3	0.512882	2	4.92	0.283073	5	10.18	18.5897	13	15.6074	15	38.4966	46
CL 010	Villarrica	0.704019	3	0.512884	3	4.96	0.283074	6	10.23	18.5882	9	15.6077	9	38.4963	29
CL 166	Villarrica	0.703932	3	0.512862	2	4.52	0.283068	8	10.01	18.6145	10	15.6094	10	38.5165	32
CL 170	Villarrica	0.704022	3	0.512894	2	5.16				18.5896	8	15.6078	9	38.4960	29
CL 017*	Huilemolle*	0.703892	3	0.512834	3	3.99				18.5662	17	15.6033	21	38.4635	68
CL 022*	Caburga*	0.703739	2	0.512854	3	4.36	0.283038	5	8.95	18.5873	12	15.6028	12	38.4712	36
CL159	Mocho	0.704067	3	0.512833	1	3.96	0.283032	5	8.72	18.5913	4	15.6084	4	38.4999	11
CL161	Mocho	0.704102	3	0.512828	2	3.86				18.5908	11	15.6079	11	38.5007	32
CL 109	Casablanca	0.704049	3	0.512843	3	4.15	0.283037	6	8.92	18.5836	12	15.6072	15	38.4792	47
CL109_rep		*0.704054*	*3*	*0.512842*	*2*	*4.14*				*18.5873*	*12*	*15.6133*	*10*	*38.5018*	*26*
CL 701	Casablanca	0.703941	3	0.512832	3	3.93	0.283020	6	8.31	18.5786	21	15.6043	26	38.4686	86
CL 088*	Cabeza de Vaca*	0.703780	3	0.512839	2	4.08				18.5461	10	15.5958	11	38.4015	35
CL 098	Osorno	0.704300	2	0.512806	3	3.43	0.283014	4	8.12	18.6107	9	15.6112	8	38.5195	23
CL 102	Osorno	0.704335	3	0.512796	3	3.24				18.6148	8	15.6147	9	38.5330	26
CL 713*	Apagado*	0.703531	3	0.512896	2	5.20	0.283050	4	9.37	18.4935	7	15.5786	6	38.2728	14
CL 713_rep		*0.703523*	*3*	*0.512901*	*2*	*5.29*				*18.4916*	*13*	*15.5777*	*16*	*38.2688*	*50*
CL 443*	Chaiten*	0.703932	3	0.512807	2	3.46				18.5973	8	15.6074	10	38.4968	32
CL 486*	Chaiten*	0.704144	3	0.512787	3	3.07	0.282975	6	6.72	18.6123	8	15.6094	10	38.5105	31
CL 490*	Chaiten*	0.704163	3	0.512784	3	3.00	0.282974	6	6.69	18.6118	11	15.6073	12	38.5040	39
Backarc															
CL 425	old plateau basalt	0.703887	3	0.512794	2	3.20	0.282938	4	5.41	18.5344	19	15.5980	23	38.4089	75
CL 426	Rd to Pino Hachado	0.703951	3	0.512778	2	2.89				18.5427	6	15.5997	6	38.4268	16
CL 430	old plateau basalt	0.703940	3	0.512792	2	3.17				18.5160	20	15.5869	25	38.3514	82
CL 475 b	around Laguna Blanca	0.703991	3	0.512774	3	2.81	0.282923	7	4.88	18.5688	10	15.6004	11	38.4476	30
CL 481	Cerro Horqueta	0.704297	3	0.512725	2	1.85				18.4951	10	15.5907	12	38.4105	38
CL 482	older plateau	0.703822	3	0.512836	2	4.02				18.4426	10	15.5748	12	38.2996	39
CL 433	plateau basalt / Jacobacci Volc field	0.704048	3	0.512787	3	3.06	0.282936	5	5.32	18.4791	10	15.5907	13	38.4276	41
CL 433_rep		0.704078	3	0.512782	3					18.4802	16	15.5909	19	38.4304	65
more-enriched Backarc															
CL 424	old plateau at meteorite impact site	0.704868	3	0.512643	2	0.25	0.282712	4	-2.58	18.5508	8	15.6360	8	38.5330	21
CL 431	Jacobacci Volc field	0.704351	3	0.512753	3	2.40				18.3922	15	15.5923	18	38.3765	58
CL 432	Jacobacci Volc field	0.704550	3	0.512618	3	-0.24	0.282753	6	-1.14	18.4645	7	15.6258	7	38.5156	17
CL 434	Crater Basalt Volcanic Field	0.704879	3	0.512640	2	0.19				18.3198	14	15.5898	16	38.4946	53
CL 437	Crater Basalt Volcanic Field	0.704371	3	0.512722	3	1.80	0.282866	5	2.85	18.3046	9	15.5790	9	38.4444	30

* cinder cones

Table 2

Sample number	Sample Location	$\delta^{18}O$ olivine	$\delta^{18}O$ plag	1σ	mineral	$\delta^{18}O$ groundmass	average	$\delta^{18}O$(melt) corrected	Δ(measurements -correction)
TSVZ Volcanic Arc									
CL 725	Tinguiririca#	5.07	5.77	0.10	pl	6.35		5.67	0.68
CL 725_rep						*6.27*	*6.31*		
CL 726	Tinguiririca#	5.62	6.32	0.10	pl	6.26		6.22	
CL 726_rep						*6.15*	*6.20*		
CL 196	Los Hornitos (small cone near Cerro Azul)	5.31		0.10	ol	5.88		5.91	-0.03
CL 571	San Pedro	5.24		0.05	ol			5.84	
CL 572	San Pedro (Satellite cones)	5.09		0.10	ol	5.81		5.69	0.12
CL 575b	San Pedro (Satellite cones)	5.28		0.05	ol			5.88	
CL 576	San Pedro (Satellite cones)	5.29		0.02	ol	5.96		5.89	0.07
CL 576_rep						*6.20*	*6.08*		
CL 449	Longaví	5.52		0.03	ol			6.12	
CL 531	Longaví	4.88		0.10	ol	5.42		5.48	-0.06
CL 531_rep						*5.55*	*5.49*		
CL 559	Callaqui (Satellite cones)	5.35		0.14	ol			5.95	
CL 560	Callaqui (Satellite cones)	5.20		0.10	ol			5.80	
CSVZ Volcanic Arc									
CL 029	Llaima	4.81		0.07	ol			5.41	
CL 032	Llaima	4.53		0.07	ol	5.44		5.13	0.31
CL 032_rep						*5.35*	*5.40*		
CL 006	Villarrica	4.76		0.12	ol	5.39		5.36	0.03
CL 010	Villarrica	4.70		0.05	ol	5.52		5.30	0.22
CL 166	Villarrica	4.93		0.09	ol	5.37		5.53	-0.16
CL 166_rep						*5.45*	*5.41*		
CL 022*	Caburga*	4.90		0.23	ol	5.83		5.50	0.33
CL 109	Casablanca	4.96		0.15	ol			5.56	
CL 088*	Cabeza de Vaca*	5.34		0.10	ol			5.94	
CL 098	Osorno	4.92		0.13	ol			5.52	
CL 486*	Chaiten*	5.50		0.04	ol			6.10	
CL 490*	Chaiten*	5.48		0.07	ol	6.24		6.08	0.16
CSVZ Backarc									
CL 425	old plateau basalt	5.31		0.01	ol	5.77		5.91	-0.14
CL 475 b	around Laguna Blanca	5.34		0.10	ol			5.94	
CL 433	plateau basalt / Jacobacci Volc field	5.17		0.12	ol			5.77	
More-enriched Backarc									
CL 424	old plateau at meteorite impact site	5.72		0.10	ol	6.74		6.32	0.42
CL 424_rep						*6.33*	*6.54*		
CL 432	Jacobacci Volcanic field	5.25		0.10	ol			5.85	
CL 437	Crater Basalt Volcanic Field	5.37		0.10	ol			5.97	

* cinder cones

Olivine corrected values, by subtracting 0.7 to the plagioclase value

Table 3

	AOC	SED	Slab melt *30SED:70AOC(*)*	DMM
Rb	13.7	44.7	26.4	0.050
Ba	15.6	1238	525	0.563
Th	0.173	5.70	2.87	0.008
U	0.390	3.21	2.21	0.003
Nb	2.89	4.63	0.879	0.149
Ta	-	0.350	0.067	0.010
K	5147	17483	10267	80.0
La	3.40	13.5	9.18	0.192
Ce	11.4	32.4	27.8	0.550
Pb	0.437	17.5	8.44	0.018
Pr	2.06	3.93	4.62	0.107
Sr	109	257	187	7.66
Nd	11.3	16.3	21.4	0.581
Sm	3.95	3.65	3.72	0.239
Zr	112	123	90.1	5.08
Hf	3.07	3.40	2.50	0.157
Eu	1.34	0.905	0.892	0.096
Gd	5.55	3.51	2.23	0.358
Tb	1.01	0.547	0.228	0.070
Dy	6.56	3.32	1.03	0.505
Y	40.7	18.1	4.31	2.66
Ho	1.43	0.674	0.152	0.115
Er	4.09	1.88	0.418	0.348
Tm	-	0.290	0.268	0.055
Yb	4.020	1.97	0.087	0.365
Lu	0.636	0.298	0.145	0.058
$^{87}Sr/^{86}Sr$	0.704769	0.705637	0.705318	0.703700
$^{143}Nd/^{144}Nd$	0.513153	0.512673	0.513066	0.512820
$^{206}Pb/^{204}Pb$	18.54	18.71	18.71	18.15
$^{207}Pb/^{204}Pb$	15.45	15.63	15.63	15.54
$^{208}Pb/^{204}Pb$	37.70	38.65	38.63	38.00

Table 4

			Sr	Nd	Pb
Slab	P (Gpa)	3.9			
	T (°C)	844			
AOC	Melting (%)	22			
	Xgar	46.7			
	Xcpx	43.8			
	Xphen	0.00			
	Xrut	1.31			
	Bulk D		0.020	0.326	0.019
SED	Melting (%)	22			
	Xgar	26.1			
	Xcpx	16.7			
	Xphen	27.8			
	Xrut	0.84			
	Bulk D		0.389	1.57	0.287
Mantle	P (Gpa)	1.9			
	T (°C)	1240			
	Slab component added (%)	2.0-6.0			
	Mantle melting (%)	1.6-5.5			
	Bulk D		0.020	0.026	0.015

Highlights:

> High fluid flux beneath the Chilean Central Southern Volcanic Zone (CSVZ), reflected in the erupted arc basalts

> Hydration of the oceanic crust and serpentinization of the underlying mantle at subducted fracture zones

> No evidence for assimilation of hydrothermally-altered plutonic crust in the arc magmas

> Higher fluid flux and higher degree of melting at the CSVZ stratovolcanoes than in the TSVZ and the CSVZ cinder cones